Refined exhumation history of the northern Sierras Pampeanas, Argentina

Stefan Löbens,[1] Edward R. Sobel,[2] Frithjof A. Bense,[1] Klaus Wemmer,[1] István Dunkl,[1] and Siegfried Siegesmund[1]

Received 7 October 2012; revised 11 March 2013; accepted 15 March 2013; published 30 May 2013.

[1] The Sierra de Aconquija and Cumbres Calchaquíes in the thick-skinned northern Sierras Pampeanas, NW Argentina present an ideal setting to investigate the tectonically and erosionally controlled exhumation and uplift history of mountain ranges using thermochronological methods. Although these ranges are located along strike of one another, their spatiotemporal evolution varies significantly. Integrating modeled cooling histories constrained by K-Ar ages of muscovite and biotite, apatite fission track data as well as (U-Th)/He measurement of zircon and apatite reveal the structural evolution of these ranges beginning in the late stage of the Paleozoic Famatinian Orogeny. Following localized rift-related exhumation in the central part of the study area and slow erosion elsewhere, growth of the modern topography commenced in the Cenozoic during Andean deformation. The main activity occurred during the late Miocene, with varying magnitudes of rock uplift, surface uplift, and exhumation in the two mountain ranges. The Cumbres Calchaquíes is characterized by a total of 5–7 km of vertical rock uplift, around 3 km of crestal surface uplift, and a maximum exhumation of 2–4 km since that time. The Sierra de Aconquija experienced 10–13 km of vertical rock uplift, ~4–5 km of peak surface uplift, and 6–8 km of exhumation since around 9 Ma. Much of this exhumation occurred along a previously poorly recognized fault. Miocene reactivation of Cretaceous rift structures may explain along-strike variations within these ranges. Dating of sedimentary samples from adjacent basins supports the evolutionary model developed for the mountain ranges.

Citation: Löbens, S., E. R. Sobel, F. A. Bense, K. Wemmer, I. Dunkl, and S. Siegesmund (2013), Refined exhumation history of the northern Sierras Pampeanas, Argentina, *Tectonics*, *32*, 453–472, doi:10.1002/tect.20038.

1. Introduction

[2] The Sierras Pampeanas in central and northwestern Argentina (Figure 1) constitute a morphotectonic province characterized by generally N-S trending mountain ranges separated by intermontane basins [e.g., *Caminos*, 1979; *González Bonorino*, 1950; *Jordan and Allmendinger*, 1986]. Their geodynamic evolution is associated with terrane accretion at the southwestern protomargin of Gondwana during different orogenic cycles in the late Proterozoic-early Paleozoic [e.g., *Pankhurst and Rapela*, 1998; *Ramos*, 1988], extensional tectonism accompanied by the development of several intracontinental rift basins during the Mesozoic [e.g., *Salfity and Marquillas*, 1981; *Uliana et al.*, 1989], and compressional Andean deformation beginning in the Eocene [e.g., *Coughlin et al.*, 1998; *Carrapa et al.*, 2005; *DeCelles et al.*, 2011]. In the northern part of Argentina, this initiated the uplift of the eastern margin of the Puna Plateau [*Isacks*, 1988; *Jordan and Alonso*, 1987]. Uplift is accompanied by sedimentation into a foreland basin to the east and southeast [*Jordan and Alonso*, 1987; *DeCelles et al.*, 2011; *Siks and Horton*, 2011]. Continuous crustal shortening generated the uplift of the mountain ranges comprising the northern Sierras Pampeanas, e.g., the Cumbres Calchaquíes and the Sierra de Aconquija (Figure 1) [e.g., *González Bonorino*, 1950; *Jordan et al.*, 1983; *Allmendinger et al.*, 1983; *Costa et al.*, 1999; *Ramos*, 1999]. However, details of the evolution of this area as well as the magnitude of uplift and exhumation and the precise timing within this region are still controversial [e.g., *Coughlin et al.*, 1998; *Ramos et al.*, 2002; *Sobel and Strecker*, 2003; *Mortimer et al.*, 2007].

[3] Since the Cumbres Calchaquíes and Sierra de Aconquija in the northern Sierras Pampeanas are located immediately along-strike of one another (Figure 1), one might assume that their evolution has been similar. In this study, we examine this assumption by greatly expanding the thermochronologic database. We find that the evolution of these ranges has varied spatially as well as temporally. Exhumation and uplift processes in compressional environments depend on the effect of erosion [*England and Molnar*, 1990]; the amount of eroded

All Supporting Information may be found in the online version of this article.

[1]Geoscience Centre, University of Göttingen, Göttingen, Germany.
[2]Department of Earth and Environmental Science, University of Potsdam, Potsdam-Golm, Germany.

Corresponding author: S. Löbens, Geoscience Centre, University of Göttingen, Goldschmidtstr, Göttingen, Germany. (stefan.loebens@geo.uni-goettingen.de)

0278-7407/13/10.1002/tect.20038

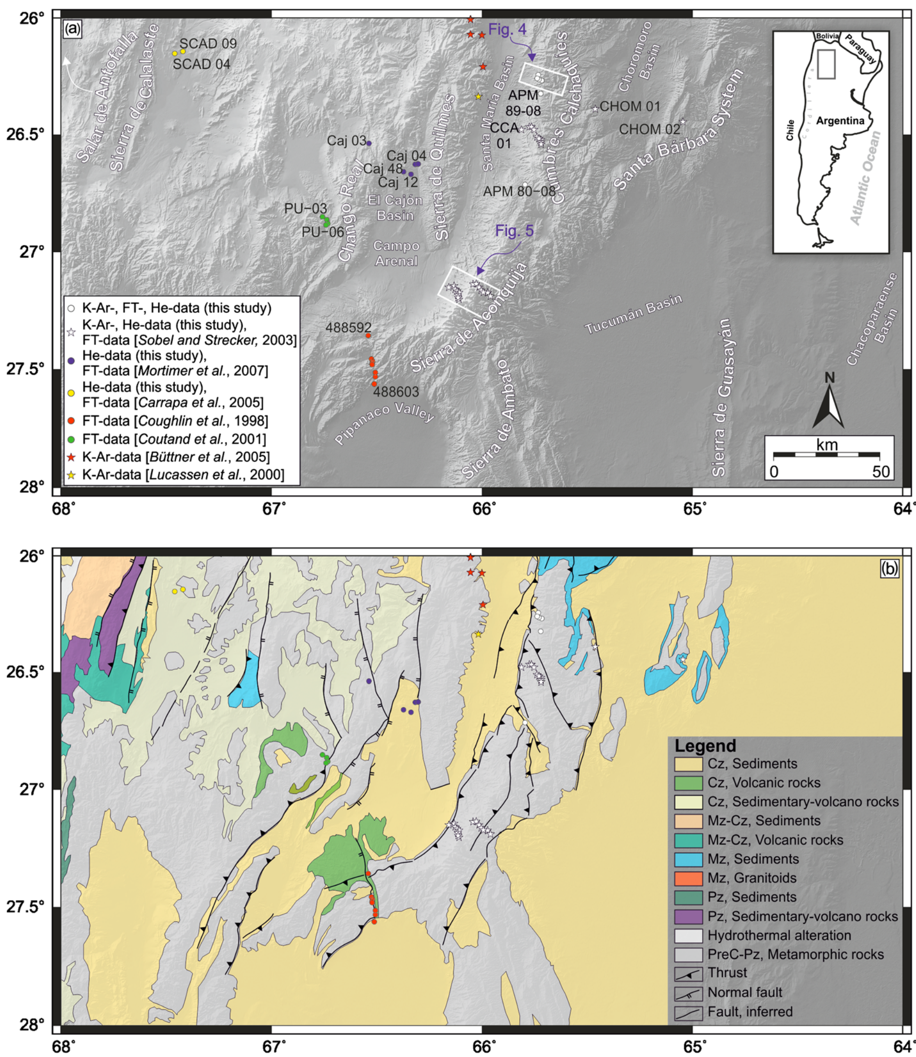

Figure 1. Overview of the study area. (a) SRTM-3 elevation model of the Northern Sierras Pampeanas including sample locations. The two white rectangles mark the main profiles in the Cumbres Calchaquíes and the Sierra de Aconquija. Sample locations from other publications which were used for comparison and interpretation are also shown; sources are listed in the inset on the left. The schematic inset in the upper right shows the location of the study area in South America. (b) Simplified geological map of the study area based on the geological maps of the provinces Catamarca, Tucumán, and Salta [*González et al.*, 1994; *Martinez*, 1995; *Salfity and Monaldi*, 1998], where Cz = Cenozoic, Mz = Mesozoic, Pz = Paleozoic, and PreC = Pre Cambrian. Scale, north direction, and sample code are the same as in Figure 1a.

material and the erosion rate are controlled by climate, climatic changes [e.g., *Beaumont et al.*, 1992; *Willett*, 1999], and lithology [e.g., *Stock and Montgomery*, 1999] as well as rock uplift [e.g., *Whittaker and Boulton*, 2012]. The locus of deformation may also be strongly influenced by preexisting structures [e.g., *González Bonorino*, 1950; *Jordan and Allmendinger*, 1986]. Due to the complex geologic history, the Sierras Pampeanas are an ideal location to test whether the influence of these different factors can be distinguished.

[4] Therefore, we used different thermochronometers in order to shed light on spatial differences in the evolution of mountain ranges within the northern Sierras Pampeanas. Conducting (1) K-Ar measurements of biotite and muscovite, (2) apatite fission track dating combined with (U-Th)/He analysis of zircon and apatite from two elevation profiles in the Sierra de Aconquija and the Cumbres Calchaquíes, (3) (U-Th)/He analysis of zircon and apatite from the surrounding area, as well as (4) integrated modeling based on these new thermochronological data allow us to explicitly reconstruct the regional cooling of these mountain ranges from approximately 420 °C to surface temperatures. Additionally, the resulting database leads to a more precise calculation of the magnitude of uplift and exhumation within these ranges. These two parameters, evolutionary history and magnitude of exhumation and uplift, are in turn the key points to resolve the differences between these two crustal-scale features within the northern Sierras Pampeanas.

2. Geologic Setting

[5] The northernmost part of the Argentine Sierras Pampeanas between 26°S-28°S and 65°W-67°W includes

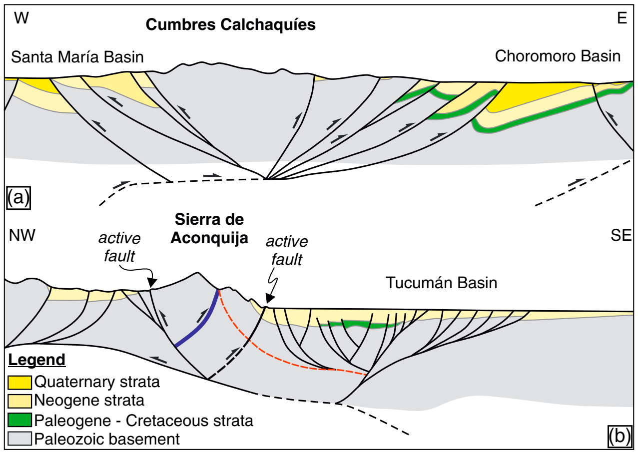

Figure 2. Schematic profile showing characteristic structures within the Northern Sierras Pampeanas. (a) Double-wedge thrusting model for the Cumbres Calchaquíes (modified from *González* [2000]) and (b) pop-up structures in the Sierra de Aconquija, based primarily on seismic reflection and earthquake data (drawn after *Cristallini et al.* [2004]). Both of these profiles exhibit questionable structural configurations, such as the singularity point in Figure 2a; the profiles are shown to illustrate the present level of uncertainty in the evolution of these basement-cored ranges. Figures are not drawn to scale. As shown in this work, at least the fault marked in red is not a correct representation of the active structures on the eastern flank of the range. Our data suggest that this geometry is best represented by the blue fault. Furthermore, it is more plausible that there are two structural systems in the profile, one represented by the Sierra de Aconquija and the other by the basin in the east.

the Sierra de Aconquija and Cumbres Calchaquíes (Figure 1). These two ranges are characterized by uplifted basement blocks with peaks up to 5000 m [e.g., *Allmendinger et al.*, 1983; *Costa et al.*, 1999; *González Bonorino*, 1950; *Jordan et al.*, 1983; *Ramos*, 1999]. Both ranges are thrust eastward and westward over the adjacent Tucumán Basin and Santa María Basin, respectively; the southern end of Cumbres Calchaquíes was also thrust over the Sierra de Aconquija along the northwest striking Amaicha Lineament, which separates the two ranges (Figure 1b) [*Allmendinger et al.*, 1983; *de Urreiztieta et al.*, 1996]. The basement of the Sierra de Aconquija and Cumbres Calchaquíes mainly consists of Precambrian metamorphic rocks intruded by the early Paleozoic Aconquija Batholith [*González Bonorino*, 1950; *Ruiz Huidobro*, 1972; *Cristallini et al.*, 2004].

[6] The Santa Bárbara system, including the Sierra de Medina, the Sierra de San Javier, and the Sierra de Ramada, is located north and east of the Sierra de Aconquija and Cumbres Calchaquíes (Figure 1a). These ranges were generated by thrusting of Cretaceous synrift deposits over Neogene sediments as a result of tectonic inversion of Cretaceous normal faults [e.g., *Abascal*, 2005; *Kley and Monaldi*, 2002; *Kley et al.*, 2005; *Ramos*, 1999].

[7] To the west, the Sierra de Aconquija and Cumbres Calchaquíes are bounded by the Santa María Basin, an intermontane basin between these ranges and the Sierra de Quilmes. Based on K/Ar data, *Linares and González* [1990] proposed a minimum age of 580 ± 20 Ma for metamorphism affecting the basement of the Sierra de Quilmes. *Büttner et al.* [2005] suggest that peak metamorphism occurred at around 470 Ma, based on U-Pb ages of monazite and titanite. Retrograde deformation ceased between 442 ± 9 Ma [*Lucassen et al.*, 2000] and approximately 410 Ma [*Büttner et al.*, 2005], constrained by Sm-Nd mineral isochrons of a mylonitic gneiss from the northeastern part of the Sierra de Quilmes as well as by K-Ar and ^{40}Ar-^{39}Ar ages of pegmatitic muscovite.

[8] During the Cretaceous, the opening of the south Atlantic resulted in extensional deformation along large areas along the trend of the Andes, leading to the development of several rifts [e.g., *Rossello and Mozetic*, 1999; *Ramos et al.*, 2002]. In the northern Pampean ranges, such a rift basin is represented by the Salta rift basin, which is characterized by up to seven depocenters where ~5000 m rift-related sediments were deposited during five evolutionary stages, three synrift stages and two postrift stages [e.g., *Ramos et al.*, 2002; *Marquillas et al.*, 2005].

[9] Subsequent exhumation, leading to formation of the basement planation surface in the northern part of the Sierra de Quilmes as well as the Sierra de Aconquija and Cumbres Calchaquíes, is indicated by apatite fission track data [*Mortimer et al.*, 2007; *Sobel and Strecker*, 2003]. These authors propose that cooling below the effective closure temperature of the apatite fission track system commenced during the Late Cretaceous, probably associated with denudation of uplifted rift shoulder areas of the Salta Rift. Subsequently, the Sierra de Aconquija and the Cumbres Clachaquíes were reheated during the middle Miocene due to burial beneath 1000–1600 m of sedimentary cover in the Santa María Basin, whereas the basement of the Sierra de Quilmes was buried beneath sediments deposited in the El Cajón-Campo del Arenal Basin.

[10] There are differences in the timing and style of subsequent exhumation and uplift of the Sierra de Aconquija and Cumbres Calchaquíes compared to the Sierra de Quilmes. The former two are bounded by high-angle active reverse faults on both sides, thus being uplifted by active double-wedge thrusting that led to development of pop-up structures at the Sierra de Aconquija (Figure 2) [*Cristallini et al.*, 2004; *Mon and Drozdzewski*, 1999; *Sobel and Strecker*, 2003]. Uplift of the two ranges along these structurally inverted faults, which are reactivated major crustal discontinuities and/or are controlled by Paleozoic basement fabrics [e.g., *Cristallini et al.*, 2004], commenced in the late Miocene-Pliocene during the latest stage of the Andean orogeny. This led to thrusting of basement and a thin cover over the adjacent Santa María and Campo del Arenal intramontane basins; thick syntectonic sediments were also synchronously deposited there (Figure 1b) [*Cristallini et al.*, 2004; *Mon and Drozdzewski*, 1999; *Sobel and Strecker*, 2003; *Strecker et al.*, 1989]. Thermal modeling of apatite fission track data and stratigraphic data suggests that exhumation and uplift of the western flanks of the Sierra de Aconquija and Cumbres Calchaquíes commenced around 6 Ma [*Sobel and Strecker*, 2003].

[11] Rather than being uplifted along a main bounding reverse fault, the Sierra de Quilmes represents a southward plunging basement anticline characterized by a complicated uplift along several reverse faults within this range and along its southeastern margin [*Cristallini et al.*, 2004; *Mortimer et al.*, 2007; *Strecker*, 1987; *Strecker et al.*, 1989]. Separating

the El Cajón-Campo del Arenal Basin from the Santa María Basin (Figure 1), the Sierra de Quilmes constitutes an out-of-sequence basement uplift which fragments a previously undisturbed foreland basin [*Mortimer et al*., 2007; *Siks and Horton*, 2011]. Based on low temperature thermochronological data and analysis of the sedimentary record of the El Cajón-Campo del Arenal Basin, these authors propose that uplift and exhumation of the Sierra de Quilmes commenced before 7–6 Ma. Furthermore, geometrical, sedimentological, and structural features of the El Cajón-Campo del Arenal Basin indicate that the range was diachronously uplifted and exhumed along its strike, beginning in the northern part [*Butz et al*., 1995; *Mortimer et al*., 2007]. Onset of the uplift and exhumation process is also implied by exhumation of a transitional range north of the Sierra de Quilmes starting between 12 Ma and 7 Ma [*Butz et al*., 1995; *Deeken et al*., 2006; *Mortimer et al*., 2007].

[12] However, as mentioned above, the interpretation of the sediments within the intramontane basins west and east of the Sierra de Aconquija and the Cumbres Clachaquíes, i.e., the Santa María and the Campo-del Arenal Basin as well as the Choromoro and Tucumán Basin, respectively, supports the evolution of the mountain ranges described by *Sobel and Strecker* [2003] and *Mortimer et al*. [2007]. The basin evolution as well as the stratigraphic record of these basins (Figure 3) is described and interpreted by several studies [e.g., *Uliana and Biddle*, 1988; *Bossi*, 1992; *Grier et al*., 1991; *Gavriloff and Bossi*, 1992; *Turner*, 1959; *Starck and Vergani*, 1996; *Kleinert and Strecker*, 2001; *Bossi et al*., 2000; *González*, 2000; *Mortimer et al*., 2007]. These authors propose that the Santa María and El Cajón-Campo del Arenal Basin are generally characterized by coarsening upward Cenozoic deposits and lack pre-Tertiary deposits (Figures 3a and 3b) [e.g., *Bossi*, 1992; *Grier et al*., 1991; *Kleinert and Strecker*, 2001], whereas the basal units overlying the Paleozoic basement in the Choromoro and Tucumán Basins are of Cretaceous age (Figures 3c and 3d) [e.g., *Turner*, 1959; *Reyes and Salfity*, 1973; *Salfity and Marquillas*, 1981; *Galliski and Viramonte*, 1988]. Correlation of at least the Cenozoic sequences of these basins, i.e., Santa María and the Campo-del Arenal Basins in the west as well as the Choromoro and Tucumán Basins to the east, suggests that a continuous sedimentary cover had formerly buried the present area of the Sierra de Aconquija and Cumbres Calchaquíes.

3. Thermochronologic Methods

[13] An effective approach to reconstructing regional cooling histories of mountain ranges below 420 °C (equivalent to approximately 21–16 km of exhumation assuming a geothermal gradient between 20 and 26 °C/km) is utilizing a combination of several thermochronometers. Typically methods include K-Ar dating of muscovite and biotite, apatite fission track (AFT), as well as (U-Th)/He dating of zircon and apatite (ZHe and AHe, respectively) [e.g., *Farley et al*., 1996].

[14] K-Ar ages are related to the effective closure temperature of the mineral phase analyzed [e.g., *Villa*, 1998; *Harrison et al*., 2009, and references therein]. Considering a grain size of ≤250 µm, these temperatures roughly range between 420–350 °C and 370–320 °C for muscovite and biotite, respectively [e.g., *Blanckenburg et al*., 1989; *Harrison et al*., 2009, and references therein].

[15] Lower temperature methods such as ZHe, AFT, and AHe constrain the final, near-surface cooling and exhumation history of a tectonic unit. Apatite fission tracks are only partially stable over geological times within a temperature interval spanning 110–60 °C for typical apatites undergoing moderate cooling rates [e.g., *Ketcham et al*., 1999; *Laslett et al*., 1987]; this range is called the partial annealing zone (PAZ_A) [e.g., *Gleadow and Fitzgerald*, 1987]. The comparable thermal window for the (U-Th)/He system is called the partial retention zone (PRZ) [e.g., *Baldwin and Lister*, 1998; *Wolf et al*., 1998] and spans 200–160 °C and 80–55 °C for zircon and apatite (PRZ_Z and PRZ_A), respectively [*Farley*, 2000; *Reiners et al*., 2004]. These temperature ranges strongly depend on the retentivity of radiogenic helium and fission tracks in the diffusion domain, i.e., the zircon and apatite crystals. This in turn is controlled by factors such as grain size, crystal morphology, alpha-damage density, and cooling rate for the (U-Th)/He system [e.g., *Ehlers and Farley*, 2003; *Reiners and Brandon*, 2006; *Wolf et al*., 1996]. For the AFT system, the retention of fission tracks mainly depends on the cooling rate and the kinetic parameter of track annealing, which can be represented by the etch pit diameter (D_{par}) [*Donelick et al*., 1999; *Ketcham et al*., 1999; *Reiners and Brandon*, 2006].

[16] In this study, basement samples from the Sierra de Aconquija, the Cumbres Calchaquíes, the Santa Bárbara System, the Sierra de Calalaste, and Sierra de Quilmes, as well as sediment samples from the El Cajón-Campo del Arenal Basin were analyzed using at least one of the methods mentioned above. (1) Due to unsuitable grain sizes of muscovite and biotite, only three samples from the Sierra de Aconquija could be dated using the K-Ar dating method (Figure 1). (2) Apatite fission track dating was applied to three basement samples from a profile in the Cumbres Calchaquíes and to ten basement samples from the eastern side of the Sierra de Aconquija (Figure 1). (3) All basement samples as well as four sediment samples (Figure 1) were analyzed using the ZHe and AHe method. The corresponding apatite fission track data for samples from the Sierra de Aconquija, the Sierra de Quilmes, the El Cajón-Campo del Arenal Basin, and the Sierra de Calalaste are published in *Sobel and Strecker* [2003], *Mortimer et al*. [2007], and *Carrapa et al*. [2005], respectively. The sample treatment and preparation used during the analytical procedure are described in detail by *Wemmer* [1991] for the K-Ar dating, by *Löbens et al*. [2011] for the (U-Th)/He dating and the Cumbres Calchaquíes AFT samples, and by *Sobel and Strecker* [2003] for the Aconquija AFT samples.

4. Results

4.1. K-Ar Cooling Ages

[17] In general, K-Ar ages from the Sierra de Aconquija show that regional cooling below 420–320 °C occurred between the Middle Ordovician and the Carboniferous (Table 1; data repository). Both the biotite and muscovite ages increase toward the NE: from 321.3 ± 5.6 Ma (ACON 28) to 466.9 ± 6.8 Ma (APM 80-08) and from 272.7 ± 4.1 Ma (ACON 29) to 476.5 ± 10.0 Ma (APM 80-08), respectively.

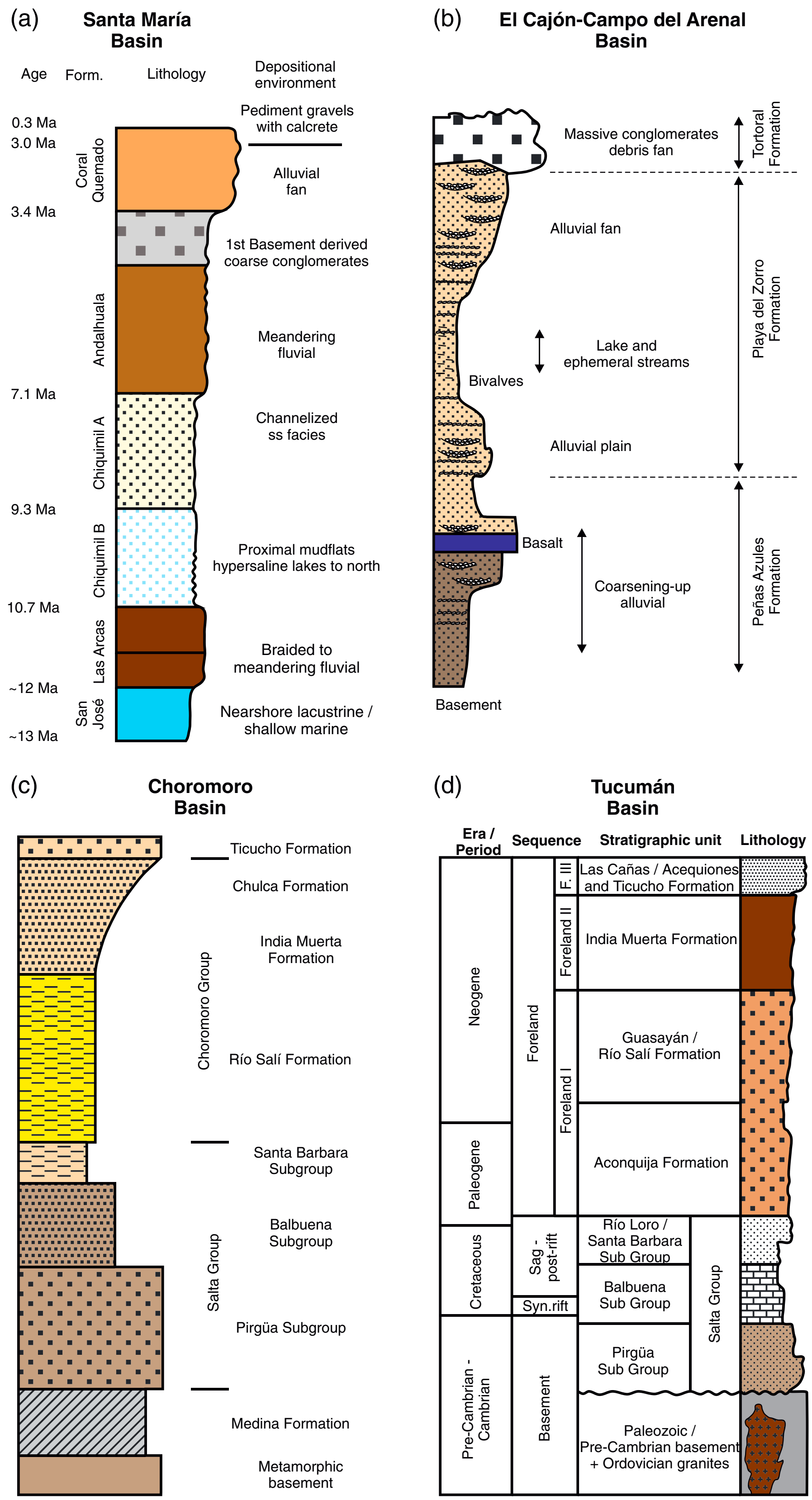

Figure 3. Schematic sketch of the stratigraphic sequences within the different basins bounding the basement ranges. (a) Santa María Basin (modified from *Kleinert and Strecker* [2001], *Bossi et al*. [2001], and *Sobel and Strecker* [2003]); (b) El Cajón-Campo del Arenal Basin (modified from *Mortimer et al*. [2007]); (c) Choromoro Basin (modified from *Abascal* [2005]); and (d) Tucumán Basin (modified from *Iaffa et al*. [2011]).

Table 1. Compilation of Ages Obtained by Different Thermochronometers[a]

			K-Ar				Zircon (U-Th)/He		Apatite Fission Track			Apatite (U-Th)/He	
			Muscovite		Biotite								
Sample	Latitude Longitude	Lithology	Age (Ma)	2σ (Ma)	Age (Ma)	2σ (Ma)	Mean Age (Ma)	2σ (Ma)	Age (Ma)	1σ (Ma)	$P(X^2)$ [%]	Mean Age (Ma)	2σ (Ma)
APM 75-08	−65.71600 −26.26900	metasediment	-	-	-	-	402.6	34.6	184.7	17.4	92.7	98.8	9.0
APM 76-08	−65.72967 −26.26417	metasediment	-	-	-	-	317.4	25.2	-	-	-	75.8	8.6
APM 78-08	−65.75567 −26.24083	metasediment	-	-	-	-	308.8	24.6	-	-	-	146.4	13.7
APM 80-08	−65.79550 −26.71317	banded schist	466.9	6.8	476.5	10.0	275.7	22.9	-	-	-	122.4	10.0
APM 87-08	−65.73183 −26.24350	metasediment	-	-	-	-	336.3	25.8	131.5	12.5	96.0	99.0	20.1
APM 88-08	−65.73733 −26.25867	metasediment	-	-	-	-	413.6	44.0	170.5	17.4	45.3	42.7	8.5
APM 89-08	−65.72083 −26.32283	metasediment	-	-	-	-	353.1	27.3	-	-	-	121.0	7.2
ACON 20	−66.04192 −27.13708	gneiss	-	-	-	-	129.6	11.1	5.9	0.8	99.9	8.4	1.0
ACON 21	−66.03865 −27.13233	metasediment	-	-	-	-	-	-	5.3	0.5	99.4	-	-
ACON 22	−66.02783 −27.13598	gneiss	-	-	-	-	-	-	4.6	0.5	96.7	-	-
ACON 23	−66.01395 −27.14985	metamorphic	-	-	-	-	-	-	4.8	0.4	97.6	-	-
ACON 24	−66.00553 −27.16203	gneiss	-	-	-	-	36.8	3.6	4.5	0.5	96.6	8.0	0.8
ACON 25	−65.99315 −27.17185	meta-volcanic	-	-	-	-	-	-	3.2	0.4	69.1	-	-
ACON 26	−65.98275 −27.17353	hyperbasal volcanic	-	-	-	-	24.0	2.0	3.3	0.4	99.4	4.1	0.6
ACON 27	−65.97652 −27.17125	gneiss	-	-	-	-	-	-	2.6	0.3	39.1	-	-
ACON 28	−65.97338 −27.17357	migmatite	321.3	5.6	272.7	4.1	9.4	0.7	2.8	0.4	64.6	3.4	0.4
ACON 29	−65.96005 −27.18837	metasediment	-	-	432.7	6.9	340.0	30.7	118.8	4.6	0	58.0	3.9
CHOM 01	−65.46170 −26.38927	metasandstone	-	-	-	-	-	-	51.8	4.3	0	-	-
CHOM 02	−65.04472 −26.44437	sandstone	-	-	-	-	321.7	23.8	212.8	6.9	0	48.8	3.4
ACON 11	−66.10835 −27.20173	metamorphic	-	-	-	-	80.5	8.3	-*	-*	-	4.4	0.5
ACON 01	−66.13283 −27.14450	metamorphic	-	-	-	-	46.7	4.1	5.1*	0.6*	-	13.7	1.2
ACB 01	−66.15833 −27.15000	granite	-	-	-	-	18.6	1.5	4.8*	0.6*	-	2.8	0.4
CCA 01	−65.81187 −26.47738	metasediment	-	-	-	-	242.6	24.9	81.6*	3.8*	-	64.9	6.0
SCAD 04	−67.46060 −26.15260	metasediment	-	-	-	-	127.5	8.3	29.0°	2.0°	-	21.5	1.8
SCAD 09	−67.42150 −26.14360	metasediment	-	-	-	-	107.2	7.6	25.8°	1.6°	-	44.3	3.8
CAJ 04	−66.30317 −26.62567	schist	-	-	-	-	254.0	19.9	81.9+	2.8+	-	72.8	15.3
CAJ 03	−66.53737 −26.53737	granite	-	-	-	-	-	-	55.4+	1.9+	-	37.3	2.7
CAJ 06	−66.30317 −26.62567	sandstone	-	-	-	-	11.8	0.8	44.2+	3.6+	-	92.6	5.6
CAJ 12	−66.33708 −26.66927	sandstone	-	-	-	-	12.3	0.8	26.8+	2.5+	-	9.0	0.9
CAJ 44	−66.31603 −26.62597	sandstone	-	-	-	-	12.0	0.7	16.0+	1.3+	-	9.7	0.7
CAJ 48	−66.37210 −26.65872	conglomerate	-	-	-	-	306.6	22.6	49.5+	2.6+	-	23.1	1.9

[a]The detailed data concerning the different thermochronometers are shown in the data repository. Ages marked by a *, °, and + are published by *Sobel and Strecker* [2003], *Carrapa et al.* [2005], and *Mortimer et al.* [2007], respectively.

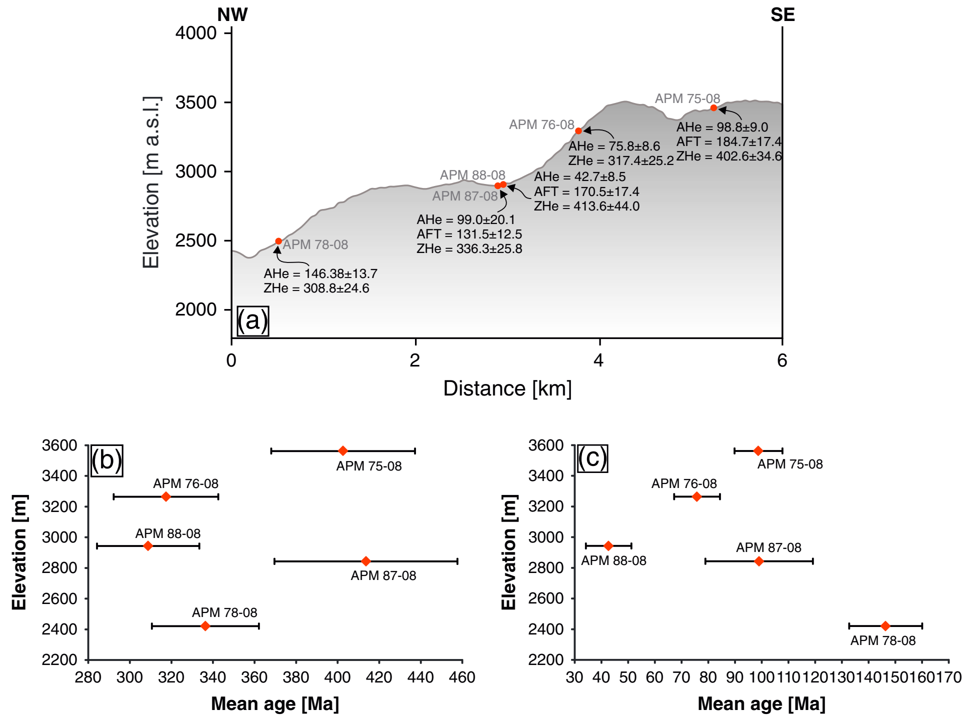

Figure 4. (a) Schematic sketch of the profile in the Cumbres Calchaquíes showing the location of samples dated by apatite and zircon (U-Th)/He method. (b and c) Age-elevation plots for the ZHe and AHe systems, respectively.

4.2. Zircon (U-Th)/He Ages

[18] Mean ZHe ages of the basement samples within the study area range from the Early Devonian to the Miocene (Table 1; data repository).

[19] The oldest ages are observed in the Cumbres Calchaquíes (Table 1; data repository), with ages between 413.6 ± 44.0 Ma (APM 88-08) and 242.6 ± 24.9 Ma (CCA 01); there is no correlation between age and elevation (Figure 4). Additionally, sample CCA 01, located at the western foot of the Cumbres Calchaquíes, has a similar ZHe age as the basement sample from the Sierra de Quilmes (CAJ 04; 254.0 ± 19.9 Ma; Table 1; data repository).

[20] ZHe ages from the Sierra de Aconquija have a broader spread than the ages from the Cumbres Calchaquíes. The former range yields ages ranging between 340.0 ± 30.7 Ma (ACON 29) and 9.4 ± 0.7 Ma (ACON 28) with a distinct positive correlation of age with elevation on both sides (Figure 5). The exception of this pattern is the bottom sample from the eastern slope (ACON 29), which is considerably older than the overlying sample (ACON 28), suggesting that a fault separates these samples.

[21] The Neogene sedimentary samples from the El Cajón-Campo Arenal Basin and the Sierra de Quilmes (CAJ 12, CAJ 44, CAJ 06) generally yield Miocene ZHe ages of ca. 12 Ma (Table 1; data repository). In contrast, CAJ 48 has a Carboniferous age (306.6 ± 22.6 Ma, Table 1; data repository).

[22] Both samples from the Sierra de Calalaste exhibit Cretaceous ages; SCAD 04 (127.5 ± 8.3 Ma), sampled at a relatively higher elevation, is slightly older than SCAD 09 (107.2 ± 7.6 Ma, Table 1; data repository).

4.3. Apatite Fission Track Ages

[23] The apparent fission track ages of the three samples from the Cumbres Calchaquíes profile range between the Jurassic (APM 75-08) and the Cretaceous (APM 87-08, Table 1; data repository). The ages correlate positively with elevation as expected for undisturbed subvertical crustal profiles (Figure 6) [*Fitzgerald et al*., 2006]. All samples are characterized by distinctly shortened tracks with a unimodal length distribution (Figure 6), with mean track lengths between 11.1 ± 1.4 µm and 11.8 ± 1.4 µm (Table 1; data repository). The mean etch pit diameter (D_{par}) of the three samples varies from 1.76 ± 0.16 µm to 1.99 ± 0.13 µm (Table 1; data repository).

[24] The fission track ages from the other Cumbres Calchaquíes profile farther south as well as from the profiles within the Sierra de Aconquija and Sierra de Quilmes (Table 1; data repository) are described in detail by *Sobel and Strecker* [2003], *Coughlin et al*. [1998], and *Mortimer et al*. [2007].

[25] Ten new samples were analyzed from a profile covering ~2400 m elevation on the eastern flank of Sierra de Aconquija. The upper nine samples yield ages between 2.8 ± 0.4 and 5.9 ± 0.8 Ma and pass the chi-squared test. The ages generally increase upward (Figure 6 and Table 1; data repository). The top of this profile is located ~9 km northeast of the top of a profile collected on the western flank of the range; AFT results from the latter are published in *Sobel and Strecker* [2003]. The AFT age of the uppermost sample of the eastern profile overlaps within error the oldest AFT ages reported from the crest of the range, suggesting that the results from the two profiles can be compared directly. The basal sample from the eastern side yields an age of 118.8 ± 4.6 Ma and fails the chi-squared test. Track lengths are moderately

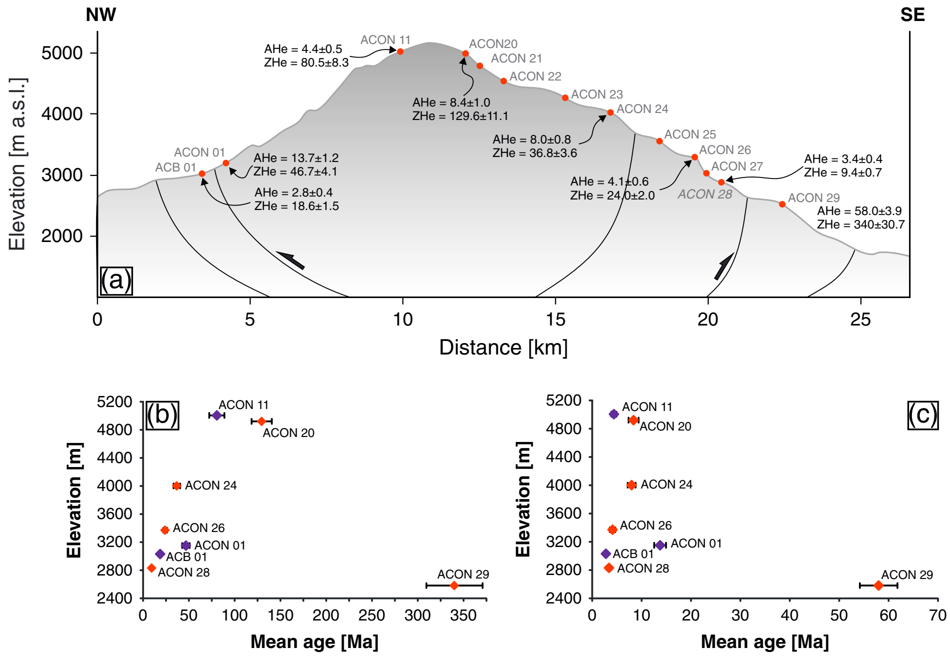

Figure 5. (a) Schematic sketch of the profile in the Sierra de Aconquija showing the location of samples dated by apatite and zircon (U-Th)/He method. (b and c) Age-elevation plots for ZHe and AHe data, respectively. Samples from the eastern flank (red diamonds) and samples from the western flank (blue diamonds).

reduced with a mean of 12.4 μm. D_{par} values for this sample are 2.2 μm, somewhat higher than the mean value of 1.8 μm obtained from the overlying nine samples. An ~N-S trending fault scarp was observed on the steep slopes between the Cretaceous-age sample and the overlying upper Neogene-age sample. This portion of the range is draped with numerous large landslides which are poorly exposed due to dense vegetation. The age pattern suggests that the scarp represents the active trace of a large, poorly mapped east vergent fault; the landslides support the contention that the fault is active.

[26] Two samples were analyzed from the western and eastern flanks of the Choromoro basin (Figure 1). The former sample, CHOM 01, collected from Paleozoic metasandstone, yields an age of 51.8 ± 4.3 Ma and has significantly shortened track lengths of 10.5 ± 0.4 μm (Table 1; data repository). The latter sample, CHOM 02, was collected from Cretaceous sandstone and yields an age of 212.8 ± 6.9 Ma and track lengths of 11.9 ± 0.2 μm (Table 1; data repository). Both samples fail the chi-squared test. CHOM 01 is partially annealed, while CHOM 02 preserves a detrital age signature.

4.4. Apatite (U-Th)/He Ages

[27] In general, the mean AHe ages of the samples, except ACON 01 and ACON 20, are younger than or coincide within the 2σ-error of the corresponding apatite fission track age (Table 1; data repository). We attribute the two anomalously old AHe ages to small inclusions in the analyzed apatite crystals rather than problems with the AFT analysis because the adjacent AFT samples yield similar ages.

[28] The mean AHe ages from Cumbres Calchaquíes vary between the Early Cretaceous (APM 89-08) and the Eocene (APM 88-08; Table 1; data repository). Within the elevation profile from the western flank of the range (samples APM 87-08 to APM 75-08; Figure 4), a distinct positive age-elevation correlation is observed, except for sample APM 87-08. This bottom sample yields an age of 99.0 ± 20.1 Ma, around 60 Ma older than APM 88-08, and nearly the same age as the top sample APM 75-08 (98.8 ± 9.0 Ma; Figure 4 and Table 1; data repository).

[29] In contrast, the samples from the Sierra de Aconquija yield considerably younger AHe ages. These ages generally range from the Miocene to the Pliocene, except for ACON 29 with an age of 58.0 ± 3.9 Ma (Table 1; data repository). There is also a positive correlation of age with elevation on both sides of the range except for samples ACON 29 and ACON 01 from the base of the eastern and western slopes, respectively (Figure 5 and Table 1; data repository).

[30] Mean AHe ages of the samples from the Sierra de Quilmes and the Sierra de Chango Real are between the Late Cretaceous (CAJ 04; 72.8 ± 15.3) and the Eocene (CAJ 03; 37.3 ± 2.7 Ma) (Table 1; data repository).

[31] Most of the sedimentary samples from the El Cajón-Campo Arenal Basin (CAJ 12, CAJ 44, CAJ 48) yield Miocene ages (Table 1; data repository) ranging between 23.1 ± 1.9 Ma (CAJ 48) and 9.0 ± 0.9 Ma (CAJ 12). In contrast, CAJ 06, which is the oldest sample stratigraphically and which is located adjacent to the basement sample CAJ 04, has a Cretaceous AHe age (92.6 ± 5.6 Ma; Table 1; data repository), suggesting that little exhumation of the ranges had occurred by this time.

[32] The two samples from the Sierra de Calalaste, SCAD 09 and SCAD 04, yield Eocene (44.3 ± 3.8 Ma) and Miocene (21.5 ± 1.8 Ma) ages, respectively (Table 1; data repository). The Eocene age is anomalously old compared to AFT ages from the same sample [*Carrapa et al.*, 2005] and therefore is disregarded.

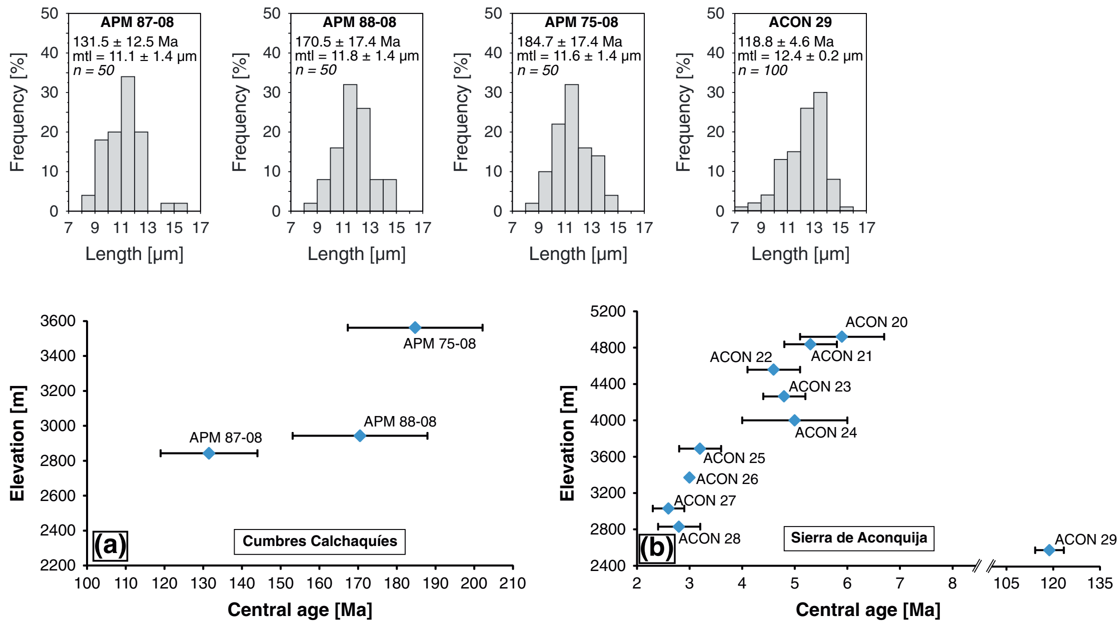

Figure 6. Age-elevation plot for the fission track data of the (a) Cumbres Calchaquíes and the (b) eastern side of the Sierra de Aconquija. Also shown is the track length distribution of the samples and their apparent age, the mean track length with standard deviation (mtl), and the number of confined tracks (*n*) measured. Due to insufficient uranium content and the young age, almost no confined tracks were detectable in the samples ACON 20-ACON 28 from the eastern side of the Sierra de Aconquija (data repository).

5. Thermal Modeling

[33] Our new thermochronological data enable the development of complete cooling paths for the individual samples from ~420 °C to surface temperature. The development of these cooling paths as well the general thermal histories of the Sierra de Aconquija and the Cumbres Calchaquíes is described and discussed in this section.

5.1. Development of Thermal Models

[34] Thermal histories of six samples (three from the Sierra de Aconquija and three from the Cumbres Calchaquíes) were modeled using the HeFTy software [*Ketcham*, 2005]. The input data for the modeling were the fission track single grain ages, track length and angular distribution, and D_{par} data as well as the corresponding (U-Th)/He ages of zircon and apatite. In order to provide models with the maximum amount of freedom to explore the model space and thereby obtain geological reasonable cooling paths, two boundary conditions were imposed on the thermal models: (1) The beginning of the time-temperature paths is constrained by the age and temperature range of the K-Ar data of muscovite and biotite, representing regional cooling below 420–320 °C [e.g., *Blanckenburg et al.*, 1989], and (2) the end is confined by the mean annual surface temperature of 17 °C [*Müller*, 1996]. For samples, where no K-Ar data exist, the age related to cooling below the closure temperature of the K-Ar systems was extrapolated from nearby samples, i.e., for ACON 20 the K-Ar age of ACON 28 was used (Table 1; data repository). Furthermore, model constraints were set as shown in Figure 7. The segments between the constraints are characterized by an episodic randomizer, a 2 times halving, and the segment path was set to be monotonic.

[35] Finally, sometimes the model solutions fit the thermochronological data but do not represent the cooling history expected from geologic observations, i.e., the sedimentary record suggests a burial reheating but the modeled cooling paths do not show this event (Figures 7c and 7d). In this case, an additional constraint, characterized by the period and maximum temperature of reheating, was set in order to force the cooling paths to go through this certain temperature at that time, thus reflecting the geologic observations (Figures 7c and 7d).

5.2. Thermal Evolution of the Basement Ranges

[36] In general, time-temperature relationships of the samples from the eastern side of the Sierra de Aconquija indicate exhumation during the Paleozoic (Figure 7). Since K-Ar ages do not exist for all samples, comparing the high temperature part of the modeled cooling history of different samples is very speculative and could be ambiguous. Therefore, only the ZHe and cooler portions of the cooling paths should be directly compared. The ZHe data indicate a relatively younger age for the presently structurally and topographically higher ACON 20 compared to ACON 29 (Figure 5). This supports the modeled high temperature cooling paths (Figures 7a–7d), suggesting that an interpolation of the K-Ar ages was, at least for ACON 20, acceptable. However, the younger ZHe age indicates either that ACON 20 was exhumed from a relatively deeper crustal level than ACON 29, hence experienced more exhumation, or that the sample was affected by a Late Paleozoic event which did not influence ACON 29. Since the ZHe ages clearly indicate a fault between ACON 29 and ACON 28 (Figure 5), it seems that ACON 20 experienced more Cenozoic exhumation than ACON 29 through thrusting, but a Late Paleozoic event cannot be completely excluded. However,

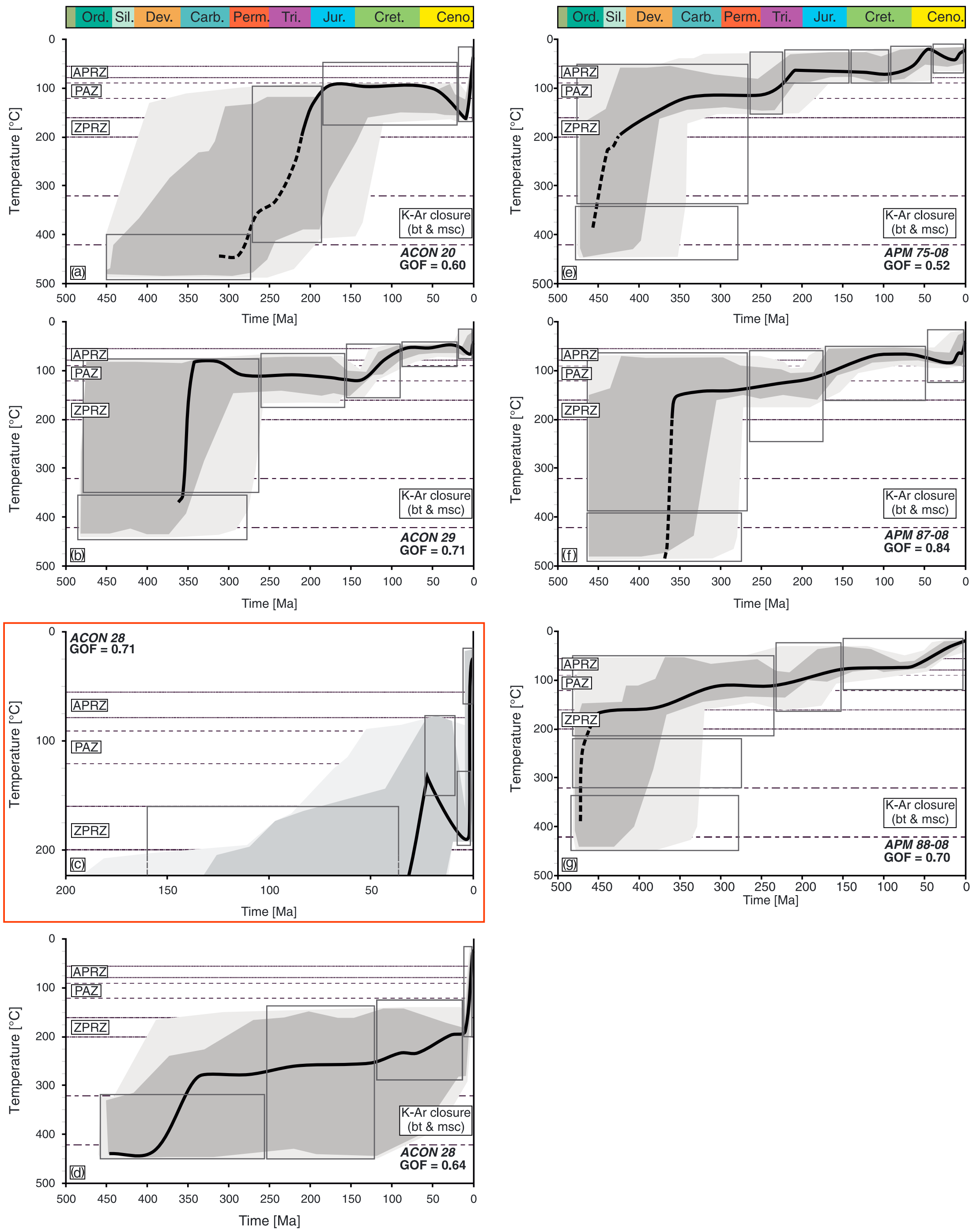

Figure 7. Cooling paths derived from thermal modeling of three samples from (a–d) Aquonquija and three samples from (e–g) Cumbres Calchaquíes. The ranges of the effective closure temperatures for the different thermochronometers and the goodness of fit (GOF) between the measured and modeled data, averaged over all input data, are shown. APRZ/ZPRZ is the partial retention zone of apatite/zircon and PAZ is the partial annealing zone of apatite. All thermal models are based on the combination of apatite fission track data and (U-Th)/He data of zircon and apatite, except for APM 87-08, where the AHe data were excluded because the single crystals were too small to get reliable ages after Ft correction (data repository). The black curve indicates the best fit, good fits are shown in dark grey, and acceptable fits in light grey. The dashed part of the best fit indicates an interpolated K-Ar age. Boxes show constraints used in the inverse models. Since the main model for ACON 28 does not show Cenozoic reheating but geologic evidence suggests that this occurred, an additional model is shown for Mesozoic to Cenozoic times (in red box). This model forces burial using an extra constraint; the good fits show that this history is plausible. Note the different x axis for this model. Ord. = Ordovician, Sil. = Silurian, Dev. = Devonian, Carb. = Carboniferous, Perm. = Permian, Tri. = Triassic, Jur. = Jurassic, Cret. = Cretaceous, Cen. = Cenozoic.

following more or less stable temperature conditions during the Mesozoic, the cooling paths for ACON 20 and 29 indicate a Miocene reheating event (Figures 7a and 7b). Since this is also suggested by the sedimentary record [e.g., *Sobel and Strecker*, 2003], but not shown the general temperature history of ACON 28 (Figure 7d), we tested a forced reheating model (Figure 7c). Both models yield good fits, showing that reheating is plausible, although the temperature of this event compared to the PRZ_Z prevents a definitive answer. However, the reheating model strongly supports the thermal history suggested by the other cooling paths from the Sierra de Aconquija and expected from the sedimentary record. Therefore, we suggest that the entire range experienced burial-driven reheating during the Miocene.

[37] In contrast, cooling below ~160 °C occurred relatively earlier during the Paleozoic in the Cumbres Calchaquíes than in the Sierra de Aconquija, excluding sample ACON 28 (Figures 7e–7g). The cooling trend of both ranges is similar during the Mesozoic, whereas the Cenozoic thermal history is again different (Figure 7). Miocene reheating in the northern part of Cumbres Calchaquíes is less pronounced (Figures 7e–7g) than in the Sierra de Aconquija. Furthermore, since there is no Cenozoic resetting of the AHe ages (Figure 4), it is arguable whether there actually was any reheating in the APM 75-08 to 88-08 profile. However, track length modeling requires reheating in the southern part of Cumbres Calchaquíes [*Sobel and Strecker*, 2003].

6. Discussion

[38] Based on the thermal models and thermochronological data, the structural evolution as well as the magnitude of Cenozoic exhumation and uplift of the Sierra de Aconquija and Cumbres Calchquíes will be discussed first. Then we address the implications of the thermochronological data from the intramontane basins and Puna Plateau to the regional evolution, completing the evolutionary history of the investigated area. Finally, all of these interpretations, especially those regarding the structural evolution of both mountain ranges, are considered in the discussion of the differences between the Sierra de Aconquija and the Cumbres Calchaquíes.

6.1. Structural Evolution of the Sierra de Aconquija

[39] Using the thermochronological data and thermal models obtained during this study, we propose a time-dependent evolutionary model for the Sierra de Aconquija commencing during the Famatinian Orogeny and lasting until present (Figure 8).

[40] The Famatinian Orogeny, related to accretion of the parautochthonous Cuyania Terrane to the southwestern margin of Gondwana during the Early Paleozoic [e.g., *Aceñolanza and Toselli*, 1988; *Baldis et al*., 1989], likely generated significant relief in the area of the present northern Sierras Pampeanas. The spatiotemporal pattern of cooling across this area can be used to decipher this evolution. Initial exhumation below ~420 °C within the region of the Sierra de Aconquija commenced during the late stage of this orogenic phase, between the Devonian and Carboniferous (Figures 7 and 8a). Since most of the Famatinian deformation was probably accommodated by a listric thrust east of the present mountain range (Figure 8a), there could have been more exhumation and rock uplift in the vicinity of sample ACON 29 compared to the area farther west (ACON 20 to ACON 28; Figure 8a). This may have led the eastern area to be uplifted to a relatively higher crustal level, with temperatures indicative of the lower boundary of the PAZ_A (approximately 60 °C; Figures 7 and 8a). In contrast, erosion was less effective on the western side; hence, exhumation of samples ACON 20 to ACON 28 occurred just below the lower boundary of the PRZ_Z (Figures 7 and 8a). Therefore, the Paleozoic sample configuration was different from the present configuration, i.e., ACON 29 was in a relatively higher position than the other samples and farther apart horizontally.

[41] Continuous cooling and hence erosion during the Mesozoic (Figure 7) caused a further reduction of the existing relief, resulting in exhumation below the upper temperature boundaries of the PAZ_A and the PRZ_A in the western and eastern parts of the Sierra de Aconquija, respectively (Figure 8b). Since the thermal models show that cooling occurred at a rate of ~0.2 °C/Ma during this interval, the total erosion was presumably quite limited. This might be related to either reduced relief where erosional processes were less effective or to a change in outcrop lithologies to ones more resistant to erosion [e.g.,*Dadson et al*., 2003]. Although *Carignano et al*. [1999] propose humid to sub-humid conditions with intervening semiarid periods during the Early Mesozoic, a climatically driven decrease of erosional forces cannot be excluded.

[42] In the Late Mesozoic, the western area (samples ACON 20 to ACON 28) was affected by very slow cooling and exhumation (Figures 7 and 8c). This is presumably related to a low topography where erosional processes are less effective (Figure 8c) as well as to an arid climate, which is indicated by deposition of carbonates and evaporates during this period [e.g., *Marquillas et al*., 2003]. Atlantic rifting ceased in the Late Cretaceous [e.g., *Schmidt et al*., 1995], removing a potential far-field tectonic driving force; this could have limited rock uplift-driven erosion. Tectonically triggered erosion was also limited in the eastern area (ACON 29) since rifting ceased in the Late Cretaceous. But since there was a more pronounced relief created while rifting was active, erosion was slightly increased compared to the western region resulting in exhumation of ACON 29 above the PRZ_A during that time (Figures 7 and 8c). The resulting sedimentary flux was probably provided to the rift basin developed in the east (Figure 8c).

[43] The Cenozoic is the next important period in the evolution of the northern Sierras Pampeanas. During the Miocene, the western part (samples ACON 20 to ACON 28) experienced ~60 °C of reheating to a maximum temperature between around 160 °C for ACON 20 and almost 200 °C for ACON 28 (Figures 7 and 8d). Analogous to the western flank of the mountain range, described by *Sobel and Strecker* [2003], this reheating could be related to burial beneath foreland basin sediments. These sedimentary deposits could have been derived from deformation and exhumation of the Puna Plateau during the early stage of the Andean orogeny (Figure 8d) [e.g., *Reynolds et al*., 2000; *Mortimer et al*., 2007; *del Papa et al*., 2010]. Furthermore, the deposits are presumably represented by the Foreland I sequence in the Tucumán Basin where the lowest unit, the Paleogene-Neogene Aconquija Formation, overlies Cretaceous strata [*Iaffa et al*., 2011]. This approximately 1100–1400 m thick unit (rough calculation basing on seismic data from *Iaffa et al*. [2011]) only crops out along the eastern margin of the Sierra de Aconquija and is not

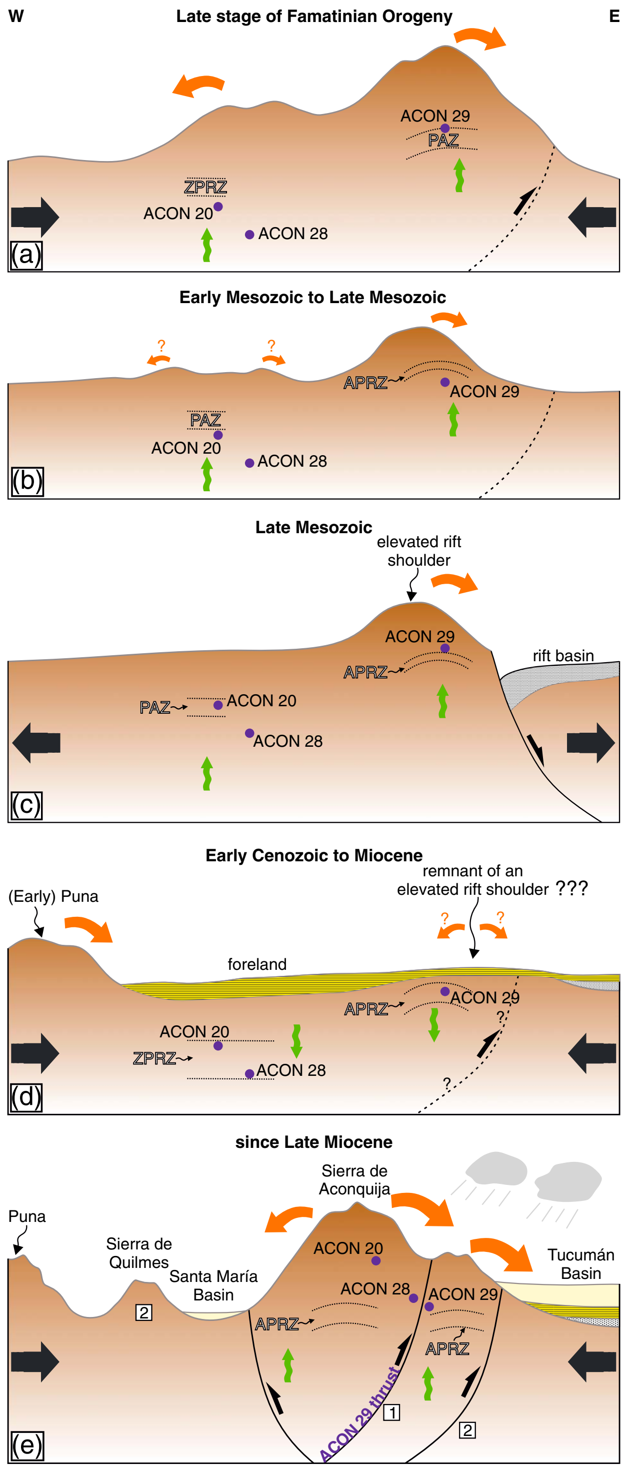

Figure 8. Schematic sketch of the structural evolution of the Sierra de Aconquija through time (vertical exaggerated) basing on the thermochronological data and the modeled time-temperature history. PAZ = partial annealing zone of apatite, APRZ/ZPRZ = partial retention zone of apatite/zircon helium thermochronometer, red arrows = intensity of erosion and direction of sediment transport, green arrows = exhumation/burial, bold black arrows = tectonic regime. Numbers indicate order of fault activity during the Late Cenozoic, including the uplift of the Sierra de Quilmes. Further details are described in the text.

documented by existing outcrops or indicated by published seismic data from the southern Santa María Basin [*Cristallini et al.*, 2004]. Although there are good seismic data in the El Cajón-Campo Arenal Basin, this unit could not be discriminated from other sequences [*Mortimer et al.*, 2007]. However, the formation might be preserved in the subsurface in these areas. Therefore, it is unclear whether deposition of this poorly dated Cenozoic unit is related to the burial reheating of samples ACON 20 to ACON 28 (Figure 7). Alternatively, the thermal model could underestimate the timing for the onset of reheating; in this case, burial heating could have commenced during the middle Miocene, as documented by the sedimentary record on the western flank of the range [*Sobel and Strecker*, 2003]. Notably, sample ACON 29, located farther east, experienced less reheating. Since the western area (around samples ACON 20 to ACON 28) was characterized by a flat topography and the eastern region in the vicinity of ACON 29 probably represented a remnant of a rift shoulder (Figure 8d) during the early Miocene, burial reheating was greater in the west than in the east after that time (Figures 7a–7d). There are little data available to constrain the source of the sediments which caused reheating (Figure 8d).

[44] In the late Miocene, the samples from the Sierra de Aconquija underwent fast cooling, hence rapid exhumation (Figure 7). The first ~1 km of exhumation is related to stripping off the sediments that formerly overlay this region [*Sobel and Strecker*, 2003]. In addition to west vergent thrusts on the western flank of the Sierra de Aconquija, deformation was accommodated by the "ACON 29 thrust" during that time (Figure 8e). As suggested by not completely reset ZHe ages, this thrust became active slightly after 9 Ma (Figures 5, 7, and 9), exhuming samples ACON 20 to ACON 28 with respect to ACON 29 and generating the present sample configuration (Figure 8e). West vergent thrusting uplifted the Sierra de Aconquija by approximately 2000 m between ca. 6 Ma and ca. 3 Ma; east vergent thrusting apparently commenced earlier and is ongoing.

[45] Therefore, cooling to surface temperatures of samples ACON 20 and ACON 28 is mainly related to the "ACON 29 thrust." Just the last approximately 70–80 °C of exhumation of these samples as well as of ACON 29 is probably caused by strong erosion controlled by a fault east of ACON 29 during the Miocene-Pliocene. Furthermore, this fault, in addition to the western main boundary fault, is still active and also generated final uplift of the mountain range (Figure 8e). Additionally, our data suggest that both the eastern and ACON 29 faults have an eastward vergence, different from that shown by *Cristallini et al*. [2004] (Figure 2b). Therefore, it is reasonable that there are two structural systems: the area of the Tucumán Basin in the east and the region of the Sierra de Aconquija, which is probably characterized by fault propagation from the west (Figure 2b). Furthermore, this interpretation contradicts the hypothesis of *Mortimer et al*. [2007] that deformation did not propagate farther into the foreland since around 6 Ma because of the uplift of the Sierra de Aconquija.

[46] Finally, since ~3 Ma, the mountain range has acted as an orographic barrier resulting in a humid climate and an arid climate on the eastern and western side, respectively (Figure 8e) [*Kleinert and Strecker*, 2001; *Sobel and Strecker*, 2003]. Therefore, erosion on the eastern flank was enhanced after ~3 Ma. This is also supported by AFT ages from the Sierra de Aconquija and the Neogene sedimentary record in the adjacent basins. Older AFT ages in the middle part of the western profile [*Sobel and Strecker*, 2003] compared to the equivalent on the eastern side (Table 1; data repository) suggest that erosion significantly slowed or even stopped at around 3 Ma on the arid western flank. This is in agreement with the absence of Neogene deposits younger than the Coral Quemado Formation in the Santa María Basin [e.g., *Bossi et al*., 1999; *Kleinert and Strecker*, 2001; *Sobel and Strecker*, 2003], while erosion probably still continued from the eastern slope into the Tucumán Basin [*Iaffa et al*., 2011].

6.2. Calculation of Cenozoic Burial and Exhumation in the Sierra de Aconquija

[47] Thermochronological data and the related thermal models of samples from the Sierra de Aconquija indicate fast cooling/re-exhumation during the late Cenozoic (Figure 7). In order to roughly calculate the magnitude of this exhumation, a geothermal gradient must be assumed. One method for combining data from multiple thermochronometers is to plot the data as a pseudovertical section [*Reiners et al*., 2003] (Figure 9). This approach assumes the geothermal gradient has remained roughly constant during cooling, suggesting the maximum possible geothermal gradient was ~35 °C/km (Figure 9, blue line). Such a gradient might have existed if heat advection related to Miocene volcanism in the Farallón Negro volcanic complex [*Sasso and Clark*, 1998] influenced samples in the Sierra de Aconquija. Although this high gradient cannot be completely excluded, it seems unlikely; otherwise, older fission track samples reported by *Coughlin et al*. [1998] would also be expected to have been reset. Therefore, a value between 20 and 26 °C/km as also used by *Sobel and Strecker* [2003] is more appropriate.

[48] Rapid cooling can cause advection of isotherms. To examine whether this is a concern at Sierra de Aconquija, the program RESPTIME [*Brandon et al*., 1998] was used with appropriate values. The results suggest that ZHe ages would have been significantly affected by advection for 1–2 Ma following the onset of cooling. This implies that the onset of cooling might have been earlier than the apparent ZHe age; however, since this age may not have been completely reset, it is difficult to constrain this onset age more precisely. This advection would also influence the precision of the pseudovertical section approach.

[49] Using the 20–26 °C/km geothermal gradient and a maximum Cenozoic reheating temperature (T_{max}) enables calculation of a maximum burial depth. Since the ZHe age of sample ACON 28, which is situated to best record the onset of cooling (Figure 5; Table 1; data repository), is strongly but not completely annealed (Figure 9), the maximum reheating temperature had to be less than 200 °C (the upper boundary of the PRZ_Z). Therefore, this sample was probably heated to as much as 170–190 °C during the Cenozoic. This agrees well with the modeled T_{max} for ACON 20, located ~2100 m higher, which had a maximal temperature of 120–160 °C (Figure 7). Assuming a paleosurface temperature of 17 °C, the maximum burial depth for sample ACON 20 was 5.5–7.2 km for a geothermal gradient between 26 and 20 °C/km.

[50] As mentioned above, Cenozoic re-exhumation of samples ACON 20 to ACON 28 commenced slightly after 9 Ma (Figure 9) through thrusting along the "ACON 29 thrust," which is presumably characterized by a listric geometry, thus generating the recent sample configuration (Figure 8e). The present vertical difference in elevation between ACON 20 and ACON 29 is ~2.5 km (data repository) and there was a temperature difference of around 100 °C between these samples at 10–9 Ma (Figure 7), which is equivalent to 3.8–5 km for the assumed geothermal gradient. Therefore, there has been a vertical offset of 6.3–7.5 km along the "ACON 29 thrust" since that time.

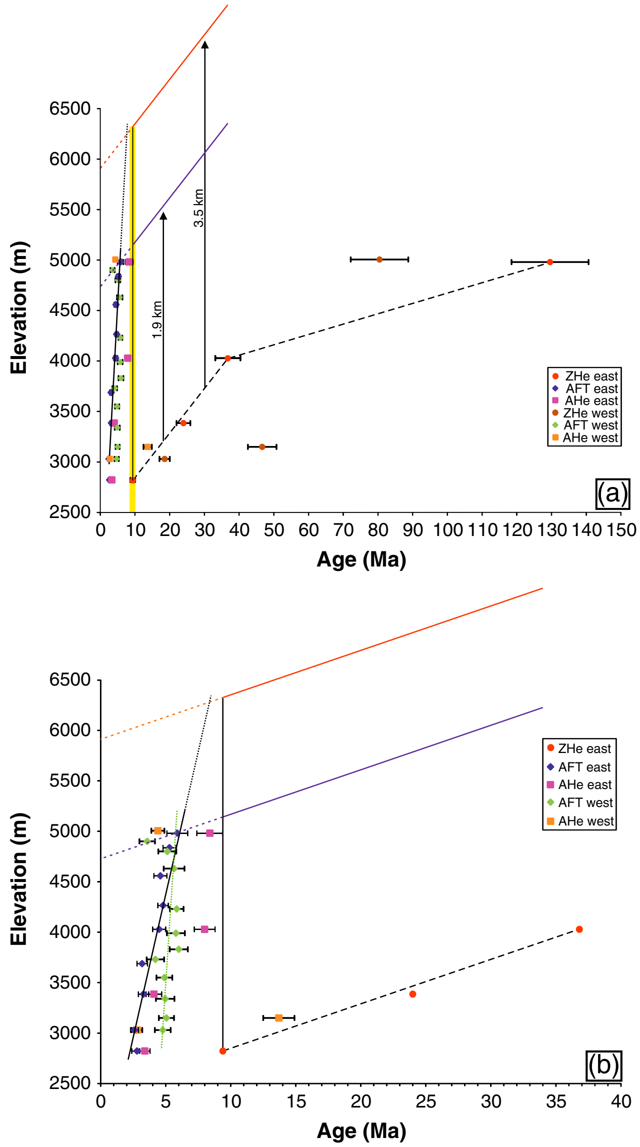

Figure 9. Age-elevation plots for samples from the Sierra de Aconquija used to estimate onset of exhumation. (a) Pseudovertical section for the zircon (U-Th)/He data and the apatite-fission track data of the Sierra de Aconquija. (b) Age-elevation plot magnifying the youngest portion of the age-elevation plot to better show the age distribution. The black dashed lines show the age-elevation path for ZHe and the black solid line and its dotted prolongation the AFT data, both from the east side of the range. We calculate the position that the ZHe curve would have if it was shifted upward to approximate an AFT cooling path. The red line shows this curve displaced upward by 3.5 km by assuming a geothermal gradient of 20 °C/km as well as a closure temperature of 180°C and 110°C for the ZHe and AFT systems, respectively. The projection of the AFT path does not directly intersect the projected ZHe curve at the age of the youngest ZHe age (9.4 Ma with the standard error marked by the thick yellow line), thus suggesting that this sample is not completely reset and cooling commenced slightly younger than 9.4 Ma. The blue line indicates minimum offset of the ZHe cooling curve, which is represented by the intersection with the highest AFT sample (ACON 20). Assuming the same closure temperatures as above, the elevation difference between this sample and ACON 28 (≈2000 m) implies a maximum geothermal gradient of ~35 °C/km, which is only plausible if Miocene volcanism in the Farallón Negro volcanic complex affected the transect location.

[51] Sample ACON 20 is now at an elevation of around 5 km above sea level (asl) and was at depth of 6–8 km below the surface at ~9 Ma. This area was at sea level at 12–13 Ma [e.g., *Gavriloff and Bossi*, 1992] and presumably remained lose to sea level for the subsequent 3–4 Ma. Therefore, a total vertical rock uplift of 10–13 km occurred since around 9 Ma, suggesting a long-term rate of 1.2–1.4 mm/a. These values agree well with the rate calculated by *Sobel and Strecker* [2003]. The surface uplift of the range crest was around 4–5 km and there was up to a maximum of 8 km of

exhumation since that time. Although this is a huge rock column to be eroded, we propose that tectonic erosion related to the uplift of the Sierra de Aconquija as well as climatically enhanced erosion on the eastern side of the range since ~3 Ma facilitated this exhumation. Furthermore, post-Cretaceous sediment thicknesses of up to 4 km and 7 km in the adjacent Santa María Basin [*González*, 2000] and Tucumán Basin [*Iaffa et al.*, 2011], respectively, support this interpretation.

6.3. Structural Evolution of the Cumbres Calchaquíes

[52] Beside the general similarities in the evolution of the Cumbres Calchaquíes to the Sierra de Aconquija (Figure 8; discussed above), there are two important differences: (1) the geodynamic evolution during the Paleozoic, i.e., cooling below ~420 °C; and (2) the evolutionary history during the Cenozoic.

[53] 1. Initial cooling below ~420 °C in the Cumbres Calchaquíes occurred earlier in the Paleozoic than in the Sierra de Aconquija (Figure 7). Presumably, deformation was primarily accommodated by faults bounding the Cumbres Calchaquíes during the Famatinian Orogeny before the orogenic phase affected the area of the Sierra de Aconquija. Therefore, relief and exhumation were likely generated earlier in the Cumbres Calchaquíes, at least in the area of the investigated profile.

[54] 2. In contrast to the region of the Sierra de Aconquija, the northern part of the Cumbres Calchaquíes was either not affected by Miocene reheating or was less pronounced, with a T_{max} of approximately 50–85 °C at around 15 Ma (Figures 7e and f). Such a slight reheating could be caused by deposition of a column of sediments which had a smaller thickness than in the Sierra de Aconquija. But since the cooling paths suggest continuous but very slow cooling (Figure 7g), it is more likely that the northern part of the range was partly characterized by a small positive relief and a low erosion rate (in the vicinity of APM 88-08), which is probably attributed to a fault separating this sample from the others. Furthermore, this is not only in contrast to the area of the Sierra de Aconquija but also to a transect further south in the Cumbres Calchaquíes, where burial reheating to approximately 70–91°C occurred due to burial beneath middle-late Miocene sediments [*Sobel and Strecker*, 2003]. Following this reheating, exhumation to surface temperature in both areas of the Cumbres Calchaquíes is probably caused by erosion controlled by the range bounding faults since the latest Miocene. Finally, the subsequent rock uplift and exhumation were lower in the Cumbres Calchaquíes than in the Sierra de Aconquija, as discussed below.

6.4. Calculation of Cenozoic Burial and Exhumation in the Cumbres Calchaquíes

[55] As suggested above, the northern part of Cumbres Calchaquíes was also slightly affected by Miocene reheating (Figures 7e and f). The maximum temperature reached during this time by samples APM 75-08 and APM 87-08 from the northern part of the range was around 50–85°C (Figure 7), which is significantly lower than for samples from the Sierra de Aconquija. Assuming the same geothermal gradient as for the latter, ranging from 20 to 26 °C/km, and the same paleosurface temperature (17°C), the maximum temperature of 50–85°C is equivalent to a depth of 1.2–3.4 km. This agrees well with the observed ~4 km thick sedimentary Santa María Group in the Santa María Basin to the west [*González*, 2000] and its stratigraphic equivalent in the Choromoro Basin to the east, the India Muerta Formation [*Bossi et al.*, 1999]. The erosion rate has been very low in the southern Cumbres Clachaquíes since around 3 Ma [*Sobel and Strecker*, 2003]. Considering sample APM 75-08, which is now near the crest of the range at an elevation of around 3.5 km (data repository) and was formerly at a depth of 1.2–3.4 km, a total of 4.7–6.9 km vertical rock uplift occurred since the Miocene. The crestal surface uplift was around 3 km and there has been at least 1.7–3.9 km of exhumation, primarily prior to 3 Ma. The modeled time-temperature history suggests that tectonically driven erosion during uplift of the range commenced slightly earlier than in the Sierra de Aconquija (Figure 7).

6.5. Regional Implications of Thermochronological Data from Sedimentary Basins and the Puna Plateau

[56] The thermochronological data of samples from the Sierra de Calalaste, El Cajón-Campo Arenal Basin, and Choromoro Basin generally confirm the regional cooling/exhumation history described above. Six late Oligocene-early Miocene AFT ages [*Carrapa et al.*, 2005] and one new AHe age from the Sierra de Calalaste are interpreted as reflecting exhumation associated with uplift of the early Puna; therefore, this area was characterized by positive topography in the Early Cenozoic and could provide sediments to the foreland to the east (Figure 8d) [e.g., *Carrapa et al.*, 2005; *Carrapa and DeCelles*, 2008].

[57] The thermochronological ages of the basement samples from the margins of the El Cajón-Campo Arenal Basin (CAJ 03 and CAJ 04) indicate slow exhumation of this area during the Cenozoic and Late Cretaceous (Table 2). The ZHe data from the schist sample CAJ 04 suggest that the minimum age of the metamorphic overprint here was older than 254 ± 20 Ma (Table 2). Exhumation of this sample was presumably influenced by Cretaceous rifting, whereas the slightly younger ages from sample CAJ 03 suggest that this area was less affected by this event.

[58] As the AFT data from all four sedimentary samples fail the chi-squared test, their single-grain ages were divided into four detrital populations as well as an inferred detrital volcanic population by *Mortimer et al.* [2007]. The new ZHe and AHe ages from these samples further refine depositional ages within the El Cajón-Campo Arenal Basin. The ZHe age of CAJ 06 (11.8 ± 0.8 Ma; Table 2) indicates that the zircon crystals were probably derived from synsedimentary ashes. Therefore, the depositional age is likely closer to the unweighted average ZHe age than to the depositional age of $<10.7 \pm 1.7$ Ma recommended by *Mortimer et al.* [2007] suggesting that the base of sequence 1 is older than 11 Ma. The young single grain ZHe and AHe ages farther up section represent either synsedimentary or recycled ashes; the AHe ages are typically younger. However, it is risky to draw strong conclusions from just one or two AHe crystals, so we refrain from further interpreting these results.

[59] The older AHe single-grain ages from samples CAJ 04 and CAJ 06 were likely derived from the same detrital population D4 proposed by *Mortimer et al.* [2007], which is typical of the regional basement erosion surface exposed nearby (Figure 1a, CAJ 04). In contrast

Table 2. Summary of Thermochronologic Data From the El Cajón basin and the Sierra de Quilmes[a]

Sample	Depositional Age	ZHe Ft-Corr. (Ma)	±2σ (Ma)	Unweighted Average	±2σ (Ma)	AFT (Ma)	±1σ (Ma)	$P(X^2)$ (%)	AHe Ft-Corr. (Ma)	±2σ (Ma)	Unweighted Average	±2σ (Ma)
CAJ 03	granite					55.4	1.9	7	37.3	2.7	37.3	2.7
CAJ 04	schist	255.1	19.4			81.9	2.8		64.0	21.8		
		252.8	20.2	254.0	19.9			97	81.6	8.9	72.8	15.3
CAJ 06	<10.7 ± 1.7	12.7	1.1			44.2	3.6	0	81.8	4.8		
	Seq 1	12.3	0.8						103.4	6.3	92.6	5.6
		10.8	0.7									
		11.5	0.7	11.8	0.8							
CAJ 44	<10.7 ± 1.7	13.0	0.8			16.0	1.3	0	9.6	0.8		
	Seq 1	12.4	0.7						9.9	0.6	9.7	0.7
		10.5	0.7	12.0	0.7							
CAJ 12	10.7 ± 1.7 to 5.71 ± 0.4	11.2	0.7			26.8	2.5	0	10.5	1.2		
	Seq 2	13.5	0.9	12.3	0.8				7.4	0.6	9.0	0.9
CAJ 48	<5.71 ± 0.4	285.3	21.6			49.5	2.6	0	22.8	2.0		
	Seq 4	328.0	23.7	306.6	22.6				20.6	1.9		
									25.9	1.8	23.1	1.9

[a]Deposition sequences, depositional age constraints, detrital populations, and AFT data from *Mortimer et al.* [2007]. The sedimentary sequence contains several volcanic ash layers and also reworked ashes; thus, the sampled sandstones contain young volcanically derived crystals.

to these relatively young ages, the ZHe ages from CAJ 48 (Tables 1 and 2; data repository) represent crystals that have been eroded from unreset Paleozoic units. The regional basement erosion surface around CAJ 04 is a potential source. The AHe ages from this sample are consistent with the AFT D2 path proposed by *Mortimer et al*. [2007], which could have been derived from the Sierra de Chango Real, which is located to the west-southwest along the margin of the Puna (Figure 1a). This area yields AFT ages between 38 and 29 Ma, indicative of rapid cooling [*Coutand et al*., 2001].

[60] Although the number of grains analyzed with U-Th/He is clearly insufficient to make a robust interpretation, these data serve to refine the depositional ages within the basin. The ages that do not represent ashes can be closely linked to the surrounding topography, suggesting limited transport distances.

[61] Finally, although the most eastern sample (CHOM 02) from the Choromoro Basin preserves a detrital AFT age which might be related to erosion of topography generated during the Famatinian Orogeny, at least the ages from CHOM 01 from the western part of the basin confirm our interpretation of exhumation and uplift through time (Figure 8). The AHe ages from CHOM 02 suggest that this sample resided within the PAZ_A during the Cenozoic. Since CHOM 01 is partially annealed, the sample was probably affected by burial beneath sediments during the Cretaceous to Early Cenozoic. These deposits were derived from an elevated area during that time, which could be represented by the Cumbres Calchaquíes.

6.6. Spatial Thermochronological Age Distribution in the Basement Ranges

[62] In general, the ZHe, AFT, and AHe thermochronological ages are distinctly older in the Cumbres Calchaquíes than in the Sierra de Aconquija (Figure 10). This spatial age distribution supports the evolutionary interpretation for both mountain ranges, especially the spatial differences for initial cooling below ~420°C and the temperature evolution during the Cenozoic. First, the older ZHe ages in the region of the Cumbres Calchaquíes (Figure 10a) strongly suggest that exhumation occurred earlier in this area than in the Sierra de Aconquija. As mentioned above, this is presumably related to Paleozoic relief and erosion. Second, older AFT and AHe ages within the Cumbres Calchaquíes compared to the Sierra de Aconquija (Figures 10b and 10c) are probably associated with a larger magnitude of exhumation in the latter range. The Sierra de Aconquija was affected by burial reheating to around 160°C during the Miocene, whereas T_{max} reached through reheating was characterized by the PRZ_A in the Cumbres Calchaquíes during the Miocene just resulting in a partial age reset of the AHe ages (older ages remained next to younger ages). Additionally, the very young AFT and AHe ages on the eastern flank of the Sierra de Aconquija are probably related to a humid climate, causing strong and enduring erosion in this area and resulting in relatively more young exhumation. In contrast, the western slope of the Cumbres Calchaquíes is characterized by very low erosion since at least the Pliocene, explaining the older ages.

[63] However, besides the age differences between both mountain ranges, there are also internal spatial age variations within the Cumbres Calchaquíes and the Sierra de Aconquija. These variations are probably closely associated with deformation along secondary faults mainly striking NW-SE, hence oblique to the main boundary faults within both mountain ranges (Figures 1 and 10).

[64] In the Cumbres Calchaquíes, the ages of all systems decrease toward the south from the profile investigated in this study to the cross-section described by *Sobel and Strecker* [2003] (Figure 10). We interpret this decrease in a way that the initial cooling/exhumation below ~420°C affected the whole area of the Cumbres Calchaquíes, including both profiles, and was presumably related to deformation and erosion during the latest stage of the Famatinian Orogeny, as mentioned above. During the Mesozoic, the area of the northern profile (investigated in this study) was obliquely thrust onto the area further to the south (the profile described by *Sobel and Strecker* [2003]) along a NW-SE trending fault between these cross-sections (Figures 1b and 10). Since Cretaceous strata is often associated with these NW-SE striking discontinuities [*González et al*., 1994; *Martinez*, 1995; *Salfity and Monaldi*, 1998], it is reasonable that those structures could represent pre-Cretaceous faults which were

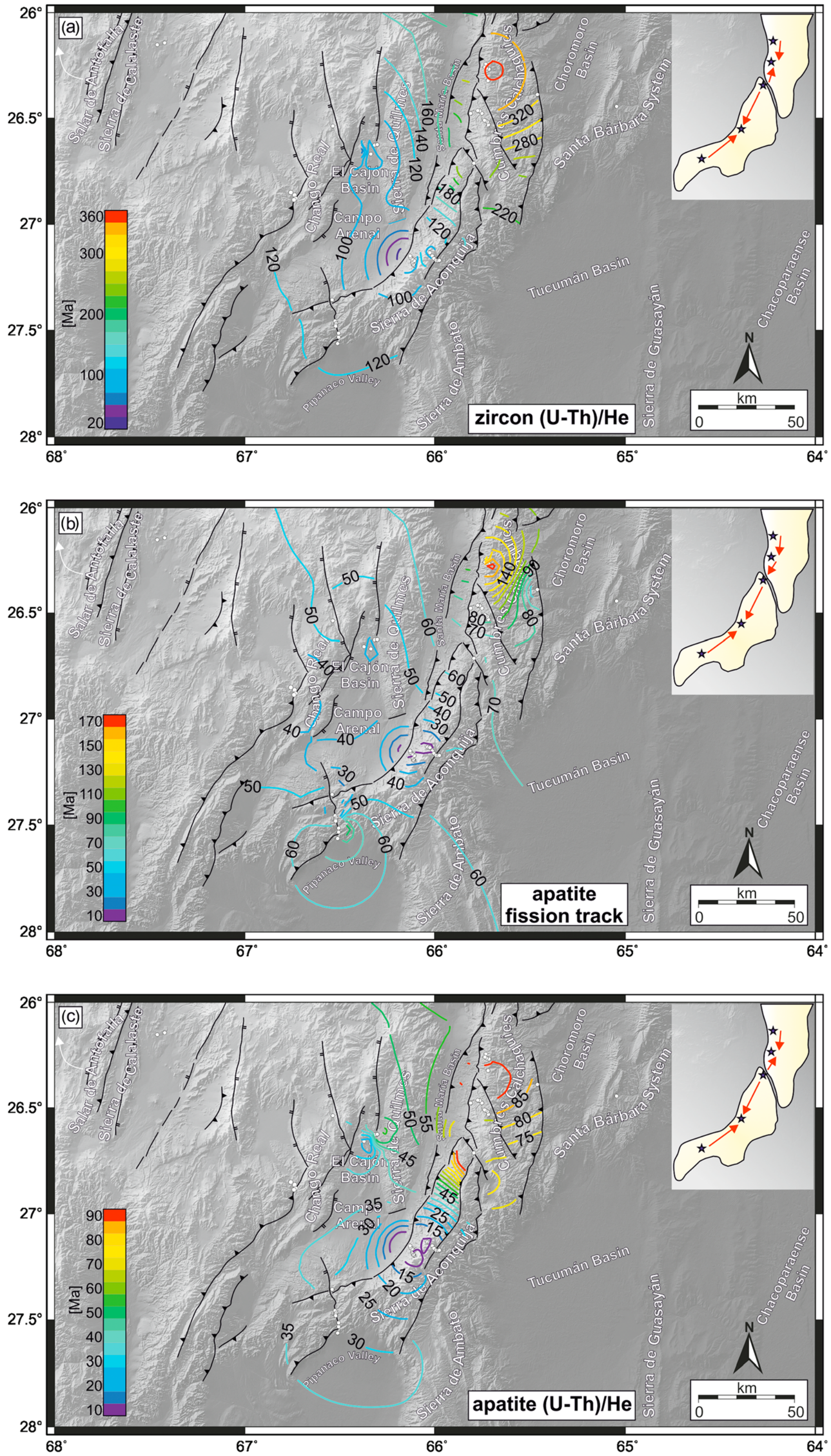

Figure 10. Lateral distribution of (a) ZHe, (b) AFT, and (c) AHe ages in the study area showing the age differences between the Cumbres Calchaquíes and the Sierra de Aconquija. The contours were generated by interpolation using the inverse distance to power method, which is implemented in the software program Surfer from Golden Software Incorporation. The interpolation was performed for the structural blocks separately; the bordering faults are indicated by black lines (sources: 1:500.000 geological maps from Salta, Tucumán, and Catamarca [*González et al.*, 1994; *Martinez*, 1995; *Salfity and Monaldi*, 1998]). In the upper right, schematic sketches show the horizontal age gradients (Ma/km) from the Cumbres Calchaquíes to the Sierra de Aconquija; morphologic changes are not considered. The blue stars mark the age cluster/point used for calculation. The red arrows indicate direction to younger ages. Age trends that are extrapolated from partially reset samples illustrate the exhumation gradient of the ranges.

reactivated as normal faults during the Cretaceous. A Cretaceous reactivation is also supported by the AHe ages of the samples from the northern profile (Figure 4). Additionally, this thrusting is presumably associated with movement along the NE-SW striking right lateral transpressional Tucumán Transfer Zone (TTZ) [*de Urreiztieta et al.*, 1996; *Gapais et al.*, 2000; *Roy et al.*, 2006]. Furthermore, the relative earlier uplift as well as the resulting enhanced erosion of the northern part of the mountain range explains the older AFT ages from this area (Figure 10b). Since the late Miocene, AHe ages from the entire Cumbres Calchaquíes suggest a uniform development, characterized by slow erosion and slow exhumation. Therefore, the observed differences in AFT ages between the northern and southern cross sections were preserved during final exhumation.

[65] In contrast to the Cumbres Calchaquíes, the spatial-temporal distribution of all thermochronometers generally varies from north to south within the Sierra de Aconquija (Figure 10). There is a decrease in age from the northern tip of the range (APM 80-08) toward minimum ages within the cross section investigated during this study followed by an increase to the profile in the SW described by *Coughlin et al.* [1998] (Figures 1 and 10). As mentioned above, the young ages on the eastern side of the middle part are related to a humid climate since at least 3 Ma causing strong erosion of the "ACON 29 thrust" hangingwall, hence continuous exhumation since that time (Figure 10). In contrast, AFT and AHe ages from the northern and southern portions of the range are partially reset and show slow cooling from the Cretaceous to Paleogene (Figures 10b and 10c). These relatively older ages are probably associated with less tectonic deformation coupled to less efficient erosion. A simple way to interpret this late Cenozoic exhumation pattern is a bow-shaped displacement pattern, with the largest amount of exhumation in the center of the structure, decreasing to either end [e.g., *Shumin and Dixon*, 1991].

7. Conclusions

[66] 1. Initial cooling and exhumation within the Sierra de Aconquija commenced during the late stage of the Famatinian Orogeny, between the Devonian and Carboniferous, which produced larger amounts of exhumation and therefore more pronounced relief in the eastern area compared to the western part. At Cumbres Calchaquíes, cooling through ~320 to ~110°C occurred relatively earlier during the Paleozoic than in the Sierra de Aconquija. Whether this was related to a Paleozoic fault between the northern and southern part of the Cumbres Calchaquíes cannot yet be solved because, to date, there are no good published data concerning Paleozoic precursors to such a structure.

[67] 2. During the Mesozoic, the western part of the Sierra de Aconquija experienced less exhumation than the eastern portion of the range, likely due to lithological and climatic differences. Very slow erosion and limited exhumation of the Cumbres Calchaquíes occurred due to an arid climate. The southern part of the Cumbres Calchaquíes was exhumed due to uplift of a Cretaceous rift-shoulder. Subsequently, exhumation continued through the Late Cretaceous to Early Cenozoic.

[68] 3. During the Cenozoic, uplift of the Early Puna triggered erosion. The resulting sediment was deposited to the east in a foreland basin, resulting in ~60°C of burial reheating in the western part of the Sierra de Aconquija and the southern part of the Cumbres Calchaquíes. However, the northern part of the Cumbres Calchaquíes and the eastern part of the Sierra de Aconquija experienced little or no burial.

[69] 4. In the late Miocene, slightly after 9 Ma, Andean deformation was accommodated by the "ACON 29 thrust" on the eastern side of the Sierra de Aconquija, resulting in significant exhumation. Displacement along this previously poorly described structure generated the present configuration of the sample sites and uplifted the range. Subsequently, deformation propagated eastward to a new range-bounding fault. Final cooling of all samples on the eastern side of the Sierra de Aconquija generally occurred synchronously. Erosion there was enhanced since ~3 Ma, when the mountain range became an orographic barrier between humid and arid areas east and west of the range, respectively. Final cooling and re-exhumation to surface temperatures of the Cumbres Calchaquíes during the Miocene are controlled by range-bounding faults accommodating NW-SE compression.

[70] 5. Overall, 10–13 km of vertical rock uplift occurred at the Sierra de Aconquija since around 9 Ma; the crestal surface uplift was around 4–5 km, and maximum exhumation was between 6 and 8 km. A total of 4.7–6.9 km vertical rock uplift occurred in the Cumbres Calchaquíes since the Late Cenozoic, whereupon the crestal surface uplift was around 3 km and the maximum exhumation was 1.7–3.9 km.

[71] 6. There is a large difference in the magnitude of Cenozoic exhumation and rock uplift between the Sierra de Aconquija and the Cumbres Calchaquíes, but differences in surface uplift are much less pronounced. One plausible explanation is that Miocene contractile reactivation of multiple NW-trending Cretaceous rift-related structures within Cumbres Calchaquíes may allow shortening to be distributed among more structures, thereby limiting the amount of exhumation. Alternatively, the northern area might be subjected to a drier climate and hence less efficient erosion or deformation in this region could be distributed between foreland structures and the Sierra de Quilmes.

[72] 7. Thermochronological data from basement and sedimentary samples from the Sierra de Calalaste, El Cajón-Campo Arenal Basin, and Choromoro Basin generally confirm the regional cooling/exhumation history of the mountain ranges.

[73] **Acknowledgments.** This research project is financed by the German Research Council (DFG project SI 438/31-1). We are grateful for help of Emilio Ahumada and Mónica López de Luchi alleviating the stay in Argentina, as well as André Steenken and Juan Antonio Palavecino assisting in the field-work. ERS acknowledges support by the Collaborative Research Center (SFB) 267, "Deformationsprozesse in den Anden" funded by the German Research Council (DFG). We acknowledge Brian Horton for his helpful review.

References

Aceñolanza, F. G., and A. J. Toselli (1988), El Sistema de Famatina, Argentina: su interpretación como orógeno de margen continental active, *V Congreso Geol. Chileno*, *1*, 55–67.

Abascal, L. del V. (2005), Combined thin-skinned and thick-skinned deformation in the central Andean foreland of northwestern Argentina, *J. South Am. Earth Sci.*, *19*(1), 75–81, doi:10.1016/j.jsames.2005.01.004.

Allmendinger, R. W., V. A. Ramos, T. E. Jordan, M. Palma, and B. L. Isacks (1983), Paleogeography and Andean structural geometry, northwest Argentina, *Tectonics*, *2*(1), 1–16.

Baldis, B. A., S. H. Peralta, and R. Villegas (1989), Esquematizaciones de una posible transcurrencia del terrane de Precordillera como fragmento continental procedente de areas pampeano-bonaerenses, *Correlaciones Geol. Univ. Nacional de Tucumán*, *5*, 81–100.

Baldwin, S. L., and G. S. Lister (1998), Thermochronology of the South Cyclades Shear Zone, Ios, Greece: Effects of ductile shear in the argon partial retention zone, *J. Geophys. Res.*, *103*(B4), 7315–7336.

Beaumont, C., P. Fullsack, and J. Hamilton (1992), Erosional control of active compressional orogens, in *Thrust Tectonics*, edited by K. R. McClay, pp. 1–18, Chapman and Hall, New York.

Blanckenburg, F., I. M. Villa, H. Baur, G. Morteani, and R. H. Steiger (1989), Time calibration of a PT-path from the Western Tauern Window, Eastern Alps: The problem of closure temperatures, *Contr. Mineral. Petrol.*, *101*(1), 1–11.

Bossi, G. (1992), Historia de subsidencia del perfi l tipo del Neogeno del Valle de Santa Maria, *IV Reunion Argentina de Sedimentol.*, *1*, 155–172.

Bossi, G. E., S. M. Georgieff, I. J. Gavriloff, L. M. Ibañez, and C. M. Muruaga (2001), Cenozoic evolution of the intramontane Santa María basin, Pampean Ranges, northwestern Argentina, *J. South Am. Earth Sci.*, *14*(7), 725–734.

Bossi, G. E., C. M. Muruaga, and I. J. C. Gavriloff (1999), Ciclo Andino, in *Geología del Noroeste Argentino*, edited by G. González Bonorino, R. Omarini, and J. Viramonte, pp. 329–360, Salta, Associación Geólogica Argentina.

Bossi, G. E., M. E. Vides, A. L. Ahumada, S. M. Georgieff, C. Muruaga, and L. M. Ibanez (2000), Analisis de las paleocorrientes y de la varianza de los componentes a tres niveles, Neogeno del Valle del Cajón, Catamarca, Argentina, *Asociación Argentina de Sedimentol. Rev.*, *7*, 23–47.

Brandon, M. T., M. K. Roden-Tice, and J. I. Garver (1998), Late Cenozoic exhumation of the Cascadia accretionary wedge in the Olympic Mountains, northwest Washington State, *Geol. Soc. Am. Bull.*, *110*, 985–1009.

Büttner, S., J. Glodny, F. Lucassen, K. Wemmer, S. Erdmann, R. Handler, and G. Franz (2005), Ordovician metamorphism and plutonism in the Sierra de Quilmes metamorphic complex: Implications for the tectonic setting of the northern Sierras Pampeanas (NW Argentina), *Lithos*, *83*(1-2), 143–181.

Butz, D. J., C. P. Foldesi, and J. H. Reynolds (1995), Provenance of the Payogastilla Group: A preliminary uplift history of the Central Andes, Salta Province, NW Argentina, *GSA Abstracts Prog.*, *27*(2), 39.

Caminos, R. (1979), Sierras Pampeanas Noroccidentales; Salta, Tuccumán, Catamarca, La Rioja y San Juan, in *Segundo Simposio de Geología Regional Argentina*, edited by J. C. Turner, pp. 225–291, Academia Nacional de Ciencias, Córdoba.

Carignano, C., M. Cioccale, and J. Rabassa (1999), Landscape antiquity of the central-eastern Sierras Pampeanas (Argentina): Geomorphological evolution since Gondwanic times, *Zeitschrift für Geomorphol.*, *118*, 245–268.

Carrapa, B., G. Adelmann, G. E. Hilley, E. Mortimer, E. R. Sobel, and M. R. Strecker (2005), Oligocene range uplift and development of plateau morphology in the southern central Andes, *Tectonics*, *24*, TC4011, doi:10.1029/2004TC001762.

Carrapa, B., and P. G. DeCelles (2008), Eocene exhumation and basin development in the Puna of northwestern Argentina, *Tectonics*, *27*, TC1015, doi:10.1029/2007TC002127.

Costa, C. H., A. D. Giaccardi, and E. F. Gonzalez Díaz (1999), Palaeolandsurfaces and neotectonic analysis in the southern Sierras Pampeanas, Argentina, in *Uplift, Erosion and Stability: Perspectives on Long-Term Landscape Development*, edited by B. Smith, W. B. Whalley, and P. A. Warke, pp. 229–238, Geol. Soc. of London, London.

Coughlin, T. J., P. B. O. Sullivan, B. P. Kohn, and R. J. Holcombe (1998), Apatite fission-track thermochronology of the Sierras Pampeanas, central western Argentina: Implications for the mechanism of plateau uplift in the Andes, *Geology*, *26*(11), 999–1002.

Coutand, I., P. Cobbold, M. de Urreiztieta, P. Gautier, A. Chauvin, D. Gapais, E. A. Rossello, and O. López-Gamund (2001), Style and history of Andean deformation, Puna plateau, northwestern Argentina, *Tectonics*, *20*(2), 210-234.

Cristallini, E. O., A. H. Comınguez, V. A. Ramos, and E. D. Mercerat (2004), Basement double-wedge thrusting in the northern Sierras Pampeanas of Argentina (27°S)—Constraints from deep seismic reflection, in *Thrust Tectonics and Hydrocarbon Systems*, edited by K. R. McClay, pp. 65–90, AAPG Memoir 82.

Dadson, S. J., et al., (2003), Links between erosion, runoff variability and seismicity in the Taiwan orogen, *Nature*, *426*, 648–651.

Deeken, A., E. R. Sobel, I. Coutand, M. Haschke, U. Riller, and M. R. Strecker (2006), Development of the southern Eastern Cordillera, NW Argentina, constrained by apatite fission track thermochronology: From early Cretaceous extension to middle Miocene shortening, *Tectonics*, *25*, TC6003, doi:10.1029/2005TC001894.

DeCelles, P. G., B. Carrapa, B. K. Horton, and G. E. Gehrels (2011), Cenozoic foreland basin system in the central Andes of northwestern Argentina: Implications for Andean geodynamics and modes of deformation, *Tectonics*, *30*, TC6013, doi:10.1029/2011TC002948.

del Papa, C., A. Kirschbaum, J. Powell, A. Brod, F. Hongn, and M. Pimentel (2010), Sedimentological, geochemical and paleontological insights applied to continental omission surfaces: A new approach for reconstructing an eocene foreland basin in NW Argentina, *J. South Am. Earth Sci.*, *29*(2), 327–345.

Donelick, R. A., R. A. Ketcham, and W. D. Carlson (1999), Variability of apatite fission-track annealing kinetics; II, Crystallographic orientation effects, *Am. Mineral.*, *84*(9), 1224–1234.

Ehlers, T. A., and K. A. Farley (2003), Apatite (U–Th)/He thermochronometry: Methods and applications to problems in tectonic and surface processes, *Earth Planet. Sci. Lett.*, *206*(1-2), 1–14.

England, P., and P. Molnar (1990), Surface uplift, uplift of rocks, and exhumation of rocks, *Geology*, *18*(12), 1173–1177.

Farley, K. A. (2000), Helium diffusion from apatite: General behavior as illustrated by Durango fluorapatite, *J. Geophys. Res.*, *105*(B2), 2903–2914.

Farley, K., R. Wolf, and L. Silver (1996), The effects of long alpha-stopping distances on (U-Th)/He ages, *Geochim. Cosmochim. Acta*, *60*(21), 4223–4229.

Fitzgerald, P., S. Baldwin, L. Webb, and P. O'Sullivan (2006), Interpretation of (U–Th)/He single grain ages from slowly cooled crustal terranes: A case study from the Transantarctic Mountains of southern Victoria Land, *Chem. Geol.*, *225*(1-2), 91–120.

Galbraith, R. F., and G. M. Laslett (1993), Statistical models for mixed fission track ages, *Nucl. Tracks Radiat. Meas.*, *21*(4), 459–470.

Galliski, M., and J. Viramonte (1988), The Cretaceous paleorift in northwestern Argentina: A petrologic approach, *J. South Am. Earth Sci.*, *1*(4), 329–342.

Gapais, D., P. R. Cobbold, O. Bourgeois, D. Rouby, and M. de Urreiztieta (2000), Tectonic significance of fault-slip data, *J. Struct. Geol.*, *22*, 881-888.

Gavriloff, I. J. C., and G. E. Bossi (1992), Revisión general, análisis facial, correlación y edad de las Formaciones San José y Río Salí (Mioceno medio), provincias de Catamarca, Tucumán y Salta, República Argentina, *Acta Geol. Lilloana*, *17*(2), 5–43.

Gleadow, A., and P. Fitzgerald (1987), Uplift history and structure of the Transantarctic Mountains: New evidence from fission track dating of basement apatites in the Dry Valleys area, southern Victoria Land, *Earth Planet. Sci. Lett.*, *82*(1-2), 1–14.

González Bonorino, F. (1950), Lagunos problemas geológicas de las Sierras Pampeanas, *Rev. de la Asociación Geol. Argentina*, *5*, 81–110.

González, O. E. (2000), Hoja Geológica 2766-II San Miguel de Tucumán, 124pp.

González, O. E., E. L. G. Barber, F. G. Aceñolaza, A. Toselli, and F. Durand (1994), Mapa Geológico de la Provincia de Tucumán, *ServicioGeológico Minero Argentino*, Buenos Aires.

Grier, M., J. Salfity, and R. Allmendinger (1991), Andean reactivation of the Cretaceous Salta rift, northwestern Argentina, *J. South Am. Earth Sci.*, *4*(4), 351–372.

Harrison, T. M., J. Célérier, A. B. Aikman, J. Hermann, M. T. Heizler (2009), Diffusion of ^{40}Ar in muscovite, *Geochim. Cosmochim. Acta*, *73*, 1039–1051.

Iaffa, D. N., F. Sàbat, D. Bello, O. Ferrer, R. Mon, and A. A. Gutierrez (2011), Tectonic inversion in a segmented foreland basin from extensional to piggy back settings: The Tucumán basin in NW Argentina, *J. South Am. Earth Sci.*, *31*(4), 457–474.

Isacks, B. L. (1988), Uplift of the Central Andean Plateau and Bending of the Bolivian Orocline, *J. Geophys. Res.*, *93*(B4), 3211–3231.

Jordan, T. E., and R. W. Allmendinger (1986), The Sierras Pampeanas of Argentina: A modern analogue of Rocky Mountain foreland deformation, *Am. J. Sci.*, *286*(10), 737-764.

Jordan, T. E., and R. N. Alonso (1987), Cenozoic stratigraphy and basin tectonics of the Andes Mountains, 20-28° south latitude, *Bulletin*, *71*.

Jordan, T. E., B. L. Isacks, R. W. Allmendinger, J. A. Brewer, V. A. Ramos, and C. J. Ando (1983), Andean tectonics related to geometry of subducted Nazca plate, *Geol. Soc. Am. Bull.*, *94*(3), 341.

Ketcham, R. A. (2005), Forward and inverse modeling of low-temperature thermochronometry Data, *Rev. Mineral. Geochem.*, *58*(1), 275–314.

Ketcham, R. A., R. A. Donelick, and W. D. Carlson (1999), Variability of apatite fission-track annealing kinetics III: Extrapolation to geological time scales, *Am. Mineral.*, *84*, 1235–1255.

Kleinert, K., and M. R. Strecker (2001), Climate change in response to orographic barrier uplift: Paleosol and stable isotope evidence from the late Neogene Santa María basin, northwestern Argentina, *Geol. Soc. Am. Bull.*, *113*(6), 728–742.

Kley, J., and C. R. Monaldi (2002), Tectonic inversion in the Santa Barbara System of the central Andean foreland thrust belt, northwestern Argentina, *Tectonics*, *21*(6), 1061, doi:10.1029/2002TC902003.

Kley, J., E. A. Rossello, C. R. Monaldi, and B. Habighorst (2005), Seismic and field evidence for selective inversion of Cretaceous normal faults, Salta rift, northwest Argentina, *Tectonophysics*, *399*(1-4), 155–172.

Laslett, G., P. Green, I. Duddy, and A. Gleadow (1987), Thermal annealing of fission tracks in apatite 2. A quantitative analysis, *Chem. Geol. Isotope Geosci. Section*, *65*(1), 1–13.

Linares, E., and R. R. González (1990), Catalogo de edades radimétricas de la República Argentina 1957–1987, *Asociación Geol. Argentina Publ. Especiales*, *19*, 1–628.

Löbens, S., F. A. Bense, K. Wemmer, I. Dunkl, C. H. Costa, P. Layer, and S. Siegesmund (2011), Exhumation and uplift of the Sierras Pampeanas: Preliminary implications from K–Ar fault gouge dating and low-T thermochronology in the Sierra de Comechingones (Argentina), *Int. J. Earth Sci. (Geol Rundsch)*, *100*(2-3), 671–694.

Lucassen, F., R. Becchio, H. Wilke, G. Franz, M. Thirlwall, J. Viramonte, and K. Wemmer (2000), Proterozoic–Paleozoic development of the basement of the Central Andes (18–26°S)—A mobile belt of the South American craton, *J. South Am. Earth Sci.*, *13*(8), 697–715.

Marquillas, R., C. del Papa, I. Sabino, and J. Heredia (2003), Prospección del límite K/T en la cuenca del Noroeste, Argentina, *Rev. de la Asociación Geol. Argentina*, *58*(2), 271–274.

Marquillas, R. A., C. Papa, and I. F. Sabino (2005), Sedimentary aspects and paleoenvironmental evolution of a rift basin: Salta Group (Cretaceous?Paleogene), northwestern Argentina, *Intl. J. Earth Sci.*, *94*(1), 94–113, doi:10.1007/s00531-004-0443-2.

Martínez, L. (Ed.) (1995) Mapa Geológico de la Provincia de Catamarca, *Servicio Geológico Minero Argentino*, Buenos Aires.

Mon, R., and G. Drozdzewski (1999), Cinturones doblevergentes en los Andes del norte argentino - Hipótesis sobre su origen, *Rev. de la Asociación Geol. Argentina*, *54*, 3–8.

Mortimer, E., B. Carrapa, I. Coutand, L. Schoenbohm, E. R. Sobel, J. Sosa Gomez, and M. R. Strecker (2007), Fragmentation of a foreland basin in response to out-of-sequence basement uplifts and structural reactivation: El Cajón-Campo del Arenal basin, NW Argentina, *Geol. Soc. Am. Bull.*, *119*(5-6), 637–653.

Müller, M. (1996), *Handbuch ausgewählter Klimastationen der Erde*, Universität Trier, FB VI, Trier.

Pankhurst, R. J., and C. W. Rapela (1998), The proto-Andean margin of Gondwana: An introduction, *Geol. Soc. London, Spec. Publ.*, *142*(1), 1–9.

Ramos, V. A. (1988), The tectonics of central Andes: 30° to 33° latitude, *Spec. Paper Geol. Soc. Am.*, *218*, 31–54.

Ramos, V. A. (1999), Las provincias geológicas del territorio argentino, in *Geología Argentina, Anales*, edited by R. Caminos, pp. 41–96, Instituto de Geología y Recursos Minerales, SEGEMAR, Buenos Aires.

Ramos V. A., E. O. Cristallini, and D. J. Pérez (2002), The Pampean flat-slab of the Central Andes, *J. South Am. Earth Sci.*, *15*(1), 59–78.

Reiners, P. W., and M. T. Brandon (2006), Using thermochronology to understand orogenic erosion, *Ann. Rev. Earth Planet. Sci.*, *34*, 419–466.

Reiners, P. W., Z. Zhou, T. A. Ehlers, C. Xu, M. T. Brandon, R. A. Donelick, and S. Nicolescu (2003), Post-orogenic evolution of the Dabie-Shan, eastern China, from (U-Th)/He and fission-track thermochronology, *Am. J. Sci.*, *303*, 489–518, doi:10.2475/ajs.303.6.489.

Reiners, P. W., T. L. Spell, S. Nicolescu, and K. A. Zanetti (2004), Zircon (U-Th)/He thermochronometry: He diffusion and comparisons with 40Ar/39Ar dating, *Geochim. Cosmochim. Acta*, *68*(8), 1857–1887.

Reyes, F. C., and J. A. Salfity (1973), Consideraciones sobre la estratigrafía del Cretácico (subgrupo Pirgüa) del noroeste argentino, *V Congreso Geol. Argentino, Carlos Paz, Actas*, *3*, 15–36.

Reynolds, J. H., C. I. Galli, R. M. Hernández, B. D. Idleman, J. M. Kotila, R. V. Hilliard, and C. W. Naeser (2000), Middle Miocene tectonic development of the Transition Zone, Salta Province, northwest Argentina: Magnetic stratigraphy from the Metán Subgroup, Sierra de González, *Geol. Soc. Am. Bull.*, *112*(11), 1736–1751.

Rossello, E., and M. E. Mozetic (1999), Caracterización estructural y significado geotectónico de los depocentros cretácicos continentales del centro-oeste argentino, 5° Simposio sobre o Cretáceo do Brasil (Rio Claro), *Boletim*, *5*, 107–113.

Roy, R., D. Cassard, P. R. Cobbold, E. A. Rossello, M. Billa, L. Bailly, and A. L. W. Lips (2006), Predictive mapping for copper-gold magmatic-hydrothermal systems in NW Argentina: Use of a regional-scale GIS, application of an expert-guided data-driven approach, and comparison with results from a continental-scale GIS, *Ore Geol. Rev.*, *29*(3-4), 260–286.

Ruiz Huidobro, O. J. (1972), Descripción geológica de la Hoja 11e, Santa Maria, Provincia de Catamarca y Tucumán., *Servicio Nacional Minero Geológico, Buenos Aires*.

Salfity J. A., and Marquillas R. A. (1981), Las unidades estratigráficas cretácicas del norte de la Argentina, in *Cuencas Sedimentarias del Jurásico y Cretácico de América del Sur*, edited by W. Volkheimer, and E. A. Musacchio, pp. 303–317, Comité Sudamericano del Jurásico y Cretácio, Buenos Aires.

Salfity, J. A., and C. R. Monaldi (1998), Mapa Geológico de la Provincia de Salta, *Servicio Geológico Minero Argentino*, Buenos Aires.

Sasso, A. M., and A. H. Clark (1998), The Farallón Negro Group, northwest Argentina: Magmatic, hydrothermal and tectonic evolution and implications for Cu-Au metallogeny in the Andean back-arc, *SEG Newslett.*, *34*, 6–18.

Schmidt, C., R. Astini, C. Costa, C. Gardini, and P. Kraemer (1995), Cretaceous rifting, alluvial fan sedimentation, and Neogene inversion, southern Sierras Pampeanas, Argentina, in *Petroleum Basins of South America*, edited by A. J. Tankard et al., pp. 341–358, Am. Assoc. of Pet. Geol., Tulsa, Okla.

Shumin, L., and J. M. Dixon (1991), Centrifuge modelling of thrust faulting: Structural variation along strike in fold-thrust belts, *Tectonophysics*, *188*, 39–62.

Siks, B. C., and B. K. Horton (2011), Growth and fragmentation of the Andean foreland basin during eastward advance of fold-thrust deformation, Puna plateau and Eastern Cordillera, northern Argentina, *Tectonics*, *30*, TC6017, doi:10.1029/2011TC002944.

Sobel, E. R., and M. R. Strecker (2003), Uplift, exhumation and precipitation: Tectonic and climatic control of Late Cenozoic landscape evolution in the northern Sierras Pampeanas, Argentina, *Basin Res.*, *15*(4), 431–451.

Starck, D., and G. Vergani (1996), Desarrollo tecto-sedimentario del Cenozoico en el sur de la Provincia de Salta-Argentina, *Congreso Geol. Argentino*, *8*, 433–452.

Stock, J. D., and D. R. Montgomery (1999), Geologic constraints on bedrock river incision using the stream power law, *J. Geophys. Res.*, *104*(B3), 4983–4993.

Strecker, M. R. (1987), Late Cenozoic landscape development, the Santa Maria Valley, northwest Argentina, Cornell University, Ithaca.

Strecker, M. R., P. Cerveny, A. L. Bloom, and D. Malizia (1989), Late Cenozoic tectonism and landscape development in the foreland of the Andes: Northern Sierras Pampeanas (26°–28°S), Argentina, *Tectonics*, *8*(3), 517.

Turner, J. C. M. (1959), Estratigrafía del cordón de Escaya y de la sierra de Rinconada (Jujuy), *Rev. de la Asociación Geol. Argentina*, *13*, 15–39.

Uliana M. A., Biddle K. T., and Cerdán J. (1989), Mesozoic extension and formation, Argentine sedimentary basins, in *Extensional Tectonics and Stratigraphy of the North Atlantic Margins*, edited by A. Tankard and H. R. Balkwill, pp. 599–614, Am. Assoc. of Pet. Geol., Tulsa, Okla.

Uliana, M. A., and K. T. Biddle (1988), Mesozoic-Cenozoic paleogeographic and geodynamic evolution of southern South America, *Rev. Brasileira de Geociencias*, *18*(2), 72–190.

de Urreiztieta, M., D. Gapais, C. Le Corre, P. R. Cobbold, and E. Rossello (1996), Cenozoic dextral transpression and basin development at the southern edge of the Puna Plateau, northwestern Argentina, *Tectonophysics*, *254* (1-2), 17–39.

Villa, I. M. (1998), Isotopic closure, *Terra Nova*, *10*(1), 42–47.

Wemmer, K. (1991), K/Ar-Alterdatierungsmöglichkeiten für retrograde Deformationsprozesse im spröden und duktilen Bereich, Beispiele aus der KTB Vorbohrung (Oberpfalz) und dem Bereich der Insubrischen Linie (N-Italien), *Göttinger Arbeiten zur Geol. und Paläontol.*, *51*, 1–61.

Whittaker, A. C., and S. J. Boulton (2012), Tectonic and climatic controls on knickpoint retreat rates and landscape response times, *J. Geophys. Res.*, *117*, F02024, doi:10.1029/2011JF002157.

Willett, S. D. (1999), Orogeny and orography: The effects of erosion on the structure of mountain belts, *J. Geophys. Res.*, *104*(B12), 28957–28981.

Wolf, R., K. Farley, and D. Kass (1998), Modeling of the temperature sensitivity of the apatite (U–Th)/He thermochronometer, *Chem. Geol.*, *148*(1-2), 105–114.

Wolf, R., K. Farley, and L. Silver (1996), Helium diffusion and low-temperature thermochronometry of apatite, *Geochim. Cosmochim. Acta*, *60*(21), 4231–4240.